

# Coupled Chemistry-Emission Model for Atomic Oxygen Green and Red-doublet Emissions in Comet C/1996 B2 Hyakutake

Anil Bhardwaj<sup>1</sup> and Susarla Raghuram

*Space Physics Laboratory, Vikram Sarabhai Space Centre, Trivandrum 695022, India.*

bhardwaj\_spl@yahoo.com, anil\_bhardwaj@vssc.gov.in,  
raghuramsusarla@gmail.com

## ABSTRACT

The green (5577 Å) and red-doublet (6300, 6364 Å) lines are prompt emissions of metastable oxygen atoms in the <sup>1</sup>S and <sup>1</sup>D states, respectively, that have been observed in several comets. The value of intensity ratio of green to red-doublet (G/R ratio) of 0.1 has been used as a benchmark to identify the parent molecule of oxygen lines as H<sub>2</sub>O. A coupled chemistry-emission model is developed to study the production and loss mechanisms of O(<sup>1</sup>S) and O(<sup>1</sup>D) atoms and the generation of red and green lines in the coma of C/1996 B2 Hyakutake. The G/R ratio depends not only on photochemistry, but also on the projected area observed for cometary coma, which is a function of the dimension of the slit used and geocentric distance of the comet. Calculations show that the contribution of photodissociation of H<sub>2</sub>O to the green (red) line emission is 30 to 70% (60 to 90%), while CO<sub>2</sub> and CO are the next potential sources contributing 25 to 50% (<5%). The ratio of the photo-production rate of O(<sup>1</sup>S) to O(<sup>1</sup>D) would be around 0.03 (± 0.01) if H<sub>2</sub>O is the main source of oxygen lines, whereas it is ~0.6 if the parent is CO<sub>2</sub>. Our calculations suggest that the yield of O(<sup>1</sup>S) production in the photodissociation of H<sub>2</sub>O cannot be larger than 1%. The model calculated radial brightness profiles of the red and green lines and G/R ratios are in good agreement with the observations made on comet Hyakutake in March 1996.

*Subject headings:* comets: general – comets: individual (C/1996 B2 Hyakutake) – Molecular processes

## 1. Introduction

The spectroscopic emissions from dissociative products in cometary coma are often used in estimating production rates of respective cometary parent species which are sublimating directly from the nucleus (Feldman et al. 2004; Combi et al. 2004). It is a known fact that at smaller (<2 AU) heliocentric distances, the inner cometary coma is dominantly composed of H<sub>2</sub>O. The infrared emissions of H<sub>2</sub>O molecule are inaccessible from ground because of strong attenuation by the terrestrial atmosphere. Since H<sub>2</sub>O does not show any spectroscopic transitions in ultraviolet or visible regions of solar spectrum, one can estimate

its abundance indirectly based on the emissions from daughter products, like OH, O and H. Thus, tracking emissions of the dissociative products of H<sub>2</sub>O has become an important diagnostic tool in estimating the production rate as well as in understanding the spatial distribution of H<sub>2</sub>O in comets (Delsemme & Combi 1976, 1979; Fink & Johnson 1984; Schultz et al. 1992; Morgenthaler et al. 2001; Furusho et al. 2006). For estimating the density distribution of H<sub>2</sub>O from the emissions of daughter species, one has to account for photochemistry and associated emission processes.

The major dissociative channel of H<sub>2</sub>O is the formation of H and OH, but a small fraction is also possible in O(<sup>3</sup>P, <sup>1</sup>S, <sup>1</sup>D) and H<sub>2</sub>. The radiative decay of metastable <sup>1</sup>D and <sup>1</sup>S states of atomic

<sup>1</sup>Corresponding author: Anil Bhardwaj,  
bhardwaj\_spl@yahoo.com,  
Tel.: +91 471 2562330; fax: +91 471 2706535.

oxygen leads to emissions at wavelengths 6300, 6364 Å (red doublet) and 5577 Å (green line), respectively. The energy levels of atomic oxygen and these forbidden transitions are shown in Figure 1. Even though these emissions are accessible from ground-based observatories, most of the times they are contaminated by telluric night sky emissions as well as emissions from other cometary species. Doppler shift of these lines, which is a function of the relative velocity of comet with respect to the Earth, offers a separation from telluric emissions provided a high resolution cometary spectrum is obtained. In most of the cometary observations it is very difficult to separate the green line in optical spectrum because of the contamination from cometary C<sub>2</sub> (1-2) P-branch band emission. The red line 6300 Å emission is also mildly contaminated by the Q-branch emission of NH<sub>2</sub> molecule, but in high resolution spectrum this can be easily resolved.

Since these atomic oxygen emissions result due to electronic transitions which are forbidden by selection rules, solar radiation cannot populate these excited states directly from the ground state via resonance fluorescence. The photodissociative excitation and electron impact excitation of neutral species containing atomic oxygen, and ion-electron dissociative recombination of O-bearing ion species, can produce these metastable states (Bhardwaj & Haider 2002). If O(<sup>1</sup>D) is not quenched by ambient cometary species, then photons at wavelengths 6300 and 6364 Å will be emitted in radiative decay to the ground <sup>3</sup>P state. Only about 5% of O(<sup>1</sup>S) atoms result in 2972 and 2958 Å emissions via direct radiative transition to the ground <sup>3</sup>P state of atomic oxygen. Around 95% of O(<sup>1</sup>S) decays to the ground state through O(<sup>1</sup>D) by emitting green line (cf. Fig. 1). This implies that if the green line emission is present in cometary coma, the red doublet emission will also be present, but the opposite is not always true. The average lifetime of O(<sup>1</sup>D) is relatively small (~110 s) compared to the lifetime of H<sub>2</sub>O molecule (~8 × 10<sup>4</sup> s) at 1 AU. The O(<sup>1</sup>S) also has a very short average lifetime of about 0.1 s. Due to the short lifetime of these metastable species, they cannot travel larger distances in cometary coma before de-exciting via radiative transitions. Hence, these emissions have been used as diagnostic tools to estimate the abundance of H<sub>2</sub>O in comets (Fink

& Johnson 1984; Magee-Sauer et al. 1990; Morgenthaler et al. 2001). The intensity of O[I] emissions, in Rayleigh, can be calculated using the following equation (Festou & Feldman 1981)

$$I = 10^{-6} \tau_p^{-1} \alpha \beta N \quad (1)$$

where  $\tau_p$  is the lifetime of excited species in seconds,  $\alpha$  is the yield of photodissociation,  $\beta$  is the branching ratio, and  $N$  is the column density of cometary species in cm<sup>-2</sup>.

In the case of red doublet (6300 and 6364 Å), since both emissions arise due to transition from the same excited state (2P<sup>4</sup> <sup>1</sup>D) to the ground triplet state (2P<sup>4</sup> <sup>3</sup>P), the intensity ratio of these two lines should be the same as that of branching ratio of corresponding transitions. Using Einstein transition probabilities, Storey & Zeippen (2000) calculated the intensity ratio of red doublet and suggested that the intensity of 6300 Å emission would be 3 times stronger than that of 6364 Å emission, and this has been observed in several comets also (Spinrad 1982; Fink & Johnson 1984; Morrison et al. 1997; Cochran & Cochran 2001; Capria et al. 2005; Furusho et al. 2006; Capria et al. 2008; Cochran 2008).

The ratio of intensity of green line to the sum of intensities of red doublet can be calculated as

$$\frac{I_{5577}}{I_{6300} + I_{6364}} = \frac{\tau_{green}^{-1} \alpha_{green} N_{green} \beta_{green}}{\tau_{red}^{-1} \alpha_{red} N_{red} (\beta_{6300} + \beta_{6364})} \quad (2)$$

If the emission intensities of oxygen lines are completely attributed to only photodissociative excitation of H<sub>2</sub>O and column densities are assumed almost same for both emissions, then the ratio of intensities of green line to red doublet is directly proportional to the ratio of  $\tau^{-1} \alpha \beta$ . Festou & Feldman (1981) reviewed these atomic oxygen emissions in comets. Based on the observation of O[I] 2972 Å emission in the IUE spectrograph of comet Bradfield (1979X), Festou & Feldman (1981) calculated the brightness profiles of red and green emissions. Festou & Feldman (1981) also calculated a theoretical value for the ratio of the intensity of green line to red doublet (hereafter refer to as the G/R ratio), which has a value of around 0.1 if H<sub>2</sub>O is the source for these O[I] emissions in cometary comae, and it is nearly 1 if the source is CO<sub>2</sub> or CO. Observations of green and red line emissions in several comets have shown that the G/R ratio

is around 0.1, suggesting that H<sub>2</sub>O is the main source of these O[I] lines. However, since no experimental cross section or yield for the production of O(<sup>1</sup>S) from H<sub>2</sub>O is available in literature, the G/R ratio has been questioned by Huestis & Slanger (2006).

Generally, the red line is more intense than the green line because the production of O(<sup>1</sup>D) via dissociative excitation of H<sub>2</sub>O is larger compared to the radiative decay of O(<sup>1</sup>S). Since the lifetime of O(<sup>1</sup>D) is larger, quenching is also a significant loss process near the nucleus. So far, the observed G/R ratio in comets is found to vary from 0.022 to 0.3 (Cochran 1984, 2008; Morrison et al. 1997; Zhang et al. 2001; Cochran & Cochran 2001; Fusho et al. 2006; Capria et al. 2005, 2008, 2010).

There are several reactions not involving H<sub>2</sub>O which can also produce these forbidden oxygen lines (Bhardwaj & Haider 2002). Among the O-bearing species, CO<sub>2</sub> and CO also have dissociative channels producing O(<sup>1</sup>D) and O(<sup>1</sup>S). However, complex O-bearing molecules (e.g., H<sub>2</sub>CO, CH<sub>3</sub>OH, HCOOH) do not produce atomic oxygen as a first dissociative product. Based on the brightness of 6300 Å emission intensity, Delsemme & Combi (1976) derived the production rate of O(<sup>1</sup>D) in comet Bennett 1970 II and suggested that the abundance of CO<sub>2</sub> is more than that of H<sub>2</sub>O. Delsemme & Combi (1979) estimated the production of O(<sup>1</sup>D) in dissociation of H<sub>2</sub>O and CO<sub>2</sub>; about 12% of H<sub>2</sub>O is dissociated into H<sub>2</sub> and O(<sup>1</sup>D), while 67% of CO<sub>2</sub> is dissociated into CO and O(<sup>1</sup>D). They suggested that a small amount of CO<sub>2</sub> can contribute much more than H<sub>2</sub>O to the red doublet emission. The model calculations of Bhardwaj & Haider (2002) showed that the production of O(<sup>1</sup>D) is largely through photodissociative excitation of H<sub>2</sub>O while the major loss mechanism in the innermost coma is quenching by H<sub>2</sub>O. Cochran & Cochran (2001), based on the observation of width of red and green lines, argued that there must be another potential source of atomic oxygen in addition to H<sub>2</sub>O, which can produce O(<sup>1</sup>S) and O(<sup>1</sup>D). Observations of the green and red lines in nine comets showed that the green line is wider than the red line (Cochran 2008), which could be because various parent sources are involved in the production of O(<sup>1</sup>S).

The model of Glinski et al. (2004) showed that the chemistry in the inner coma can pro-

duce 1% O<sub>2</sub>, which can also be a source of red and green lines. Manfroid et al. (2007) also argued, based on lightcurves, that forbidden O[I] emissions are probably contributed through dissociation sequence of CO<sub>2</sub>. Recent observation of comet 17P/Holmes showed that the G/R ratio can be even 0.3, which is the highest reported value so far: suggesting that CO<sub>2</sub> and CO abundances might be higher at the time of observation (Capria et al. 2010).

Considering various arguments based on different observations and theoretical works, we have developed a coupled chemistry-emission model to quantify various mechanisms involved in the production of red and green line emissions of atomic oxygen. We have calculated the production and loss rates, and the density profiles, of metastable O(<sup>1</sup>D) and O(<sup>1</sup>S) atoms from the O-bearing species, like H<sub>2</sub>O, CO<sub>2</sub>, and CO, and also from the dissociated products OH and O. This model is applied to comet C/1996 B2 Hyakutake, which was studied through several observations in 1996 March (Biver et al. 1999; Morrison et al. 1997; Cochran & Cochran 2001; Morgenthaler et al. 2001; Combi et al. 2005; Cochran 2008). The line-of-sight integrated brightness profiles along cometocentric distances are calculated for 5577 and 6300 Å emissions and compared with the observed profiles of Cochran (2008). We have also evaluated the role of slit dimension, used in the observation, in determining the G/R ratio. The aim of this study is to understand the processes that determine the value of G/R ratio.

## 2. Model

The neutral parent species considered in this model are H<sub>2</sub>O, CO<sub>2</sub>, and CO. We do not consider other significant O-bearing species, like H<sub>2</sub>CO, CH<sub>3</sub>OH, since their first dissociation does not lead to the formation of atomic oxygen atom; the O atom appears in subsequent photodissociation of daughter products, like OH, CO, HCO. On 1996 March 24, the H<sub>2</sub>O production rate for comet C/1996 B2 Hyakutake measured by Mumma et al. (1996) was  $1.7 \times 10^{29} \text{ s}^{-1}$ . Based on H Ly- $\alpha$  emission observation, Combi et al. (1998) measured H<sub>2</sub>O production rate as  $2.6 \times 10^{29} \text{ s}^{-1}$  on 1996 April 4. Using molecular radio line emissions, Biver et al. (1999) derived the production rates of

different species at various heliocentric distances from 1.6 to 0.3 AU. They found that around 1 AU the relative abundance of CO with respect to H<sub>2</sub>O is high ( $\sim 22\%$ ) in the comet C/1996 B2 Hyakutake.

The number density  $n_i(r)$  of  $i^{th}$  parent species at a cometocentric distance  $r$  in the coma is calculated using the following Haser's formula

$$n_i(r) = \frac{Q_p}{4\pi v_i r^2} (e^{-\beta_i/r}) \quad (3)$$

Here  $Q_p$  is the total gas production rate of the comet,  $v_i$  and  $\beta_i$  are the gas expansion velocity (taken as  $0.8 \text{ km s}^{-1}$ , Biver et al. 1999) and the scale length ( $\beta_{H_2O} = 8.2 \times 10^4 \text{ km}$ ,  $\beta_{CO_2} = 5.0 \times 10^5 \text{ km}$ , and  $\beta_{CO} = 1.4 \times 10^6 \text{ km}$ ) of the  $i^{th}$  species, respectively. The Haser model's neutral density distribution has been used in several previous studies for deriving the production rate of H<sub>2</sub>O in comets based on the intensity of 6300 Å emission (Delsemme & Combi 1976, 1979; Fink & Johnson 1984; Morgenthaler et al. 2001). In our model calculations the H<sub>2</sub>O production rate on 1996 March 30 is taken as  $2.2 \times 10^{29} \text{ s}^{-1}$ . The abundance of CO relative to H<sub>2</sub>O is taken as 22%. Since there is no report on the observation of CO<sub>2</sub> in the comet Hyakutake, we assumed its abundance as 1% relative to H<sub>2</sub>O. However, we vary CO<sub>2</sub> abundance to evaluate its effect on the green and red-doublet emissions. The calculations are made when the comet C/1996 B2 Hyakutake was at a heliocentric distance of 0.94 AU and a geocentric distance of 0.19 AU on 1996 March 30. The calculated G/R ratio on other days of the observation is also reported.

The number density of OH produced in dissociation of parent species H<sub>2</sub>O at a given cometocentric distance  $r$  is calculated using Haser's two parameter coma model

$$n_{OH}(r) = \frac{Q_P}{4\pi v r^2} \frac{\beta_P}{\beta_R - \beta_P} (e^{-\beta_P r} - e^{-\beta_R r}) \quad (4)$$

Here  $v$  is the average velocity of daughter species taken as  $1 \text{ km s}^{-1}$ , and  $\beta_P$  and  $\beta_R$  are the destruction scale lengths of the parent (H<sub>2</sub>O,  $8.2 \times 10^4 \text{ km}$ ) and daughter (OH,  $1.32 \times 10^5 \text{ km}$ ) species, respectively (Huebner et al. 1992). The solar UV-EUV flux is taken from SOLAR2000 v.2.3.6 (S2K) model of Tobiska et al. (2000) for the day 1996

March 30, which is shown in Figure 2. For comparison the solar flux used by Huebner et al. (1992) in calculating O(<sup>1</sup>D) and O(<sup>1</sup>S) production rates from various O-bearing species is also presented in the same Figure.

The primary photoelectron energy spectrum  $Q(E, r, \theta)$  is calculated by degrading solar radiation in the neutral atmosphere using

$$Q(E, r, \theta) = \sum_i \int_{\lambda} n_i(r) \sigma_i^I(\lambda) I_{\infty}(\lambda) \exp[-\tau(r, \theta, \lambda)] d\lambda \quad (5)$$

where,

$$\tau(r, \theta, \lambda) = \sum_i \sigma_i^A(\lambda) \sec \theta \int_r^{\infty} n_i(r') dr' \quad (6)$$

Here  $\sigma_i^A(\lambda)$  and  $\sigma_i^I(\lambda)$  are the absorption and ionization cross sections, respectively, of the  $i^{th}$  species at the wavelength  $\lambda$ ,  $n_i(r)$  is its neutral gas density and  $\tau(r, \theta, \lambda)$  is optical depth of the medium at the solar zenith angle  $\theta$ .  $I_{\infty}(\lambda)$  is the unattenuated solar flux at the top of atmosphere at wavelength  $\lambda$ . All calculations are made at solar zenith angle  $\theta$  of  $0^\circ$ . The total photoabsorption and photoionization cross sections of H<sub>2</sub>O, CO<sub>2</sub>, and CO are taken from the compilation of Huebner et al. (1992) (<http://amop.space.swri.edu>), and interpolated at 10 Å bins to make them compatible with the S2K solar flux wavelength bins for use in our model calculations. The total photoabsorption and photoionization cross sections for H<sub>2</sub>O, CO<sub>2</sub>, and CO are presented in Figure 3. The photochemical production rates for ionization and excitation of various species are calculated using degraded solar flux and cross sections of corresponding processes (discussed in Section 3) at different cometocentric distances.

The primary photoelectrons are degraded in cometary coma to calculate the steady state photoelectron flux using the Analytical Yield Spectrum (AYS) approach, which is based on the Monte Carlo method (Singhal & Bhardwaj 1991; Bhardwaj & Singhal 1993; Bhardwaj & Michael 1999a; Bhardwaj & Jain 2009). The AYS method of degrading electrons in the neutral atmosphere can be explained briefly in the following manner. Monoenergetic electrons incident along Z-axis in an infinite medium are degraded in collision-by-collision manner using the Monte Carlo technique. The energy and position of the primary electron

and its secondary or tertiary are recorded at the instant of an inelastic collision. The total number of inelastic events in the spatial and energy bins, after the incident electron and all its secondaries and tertiaries have been completely degraded, is used to generate numerical yield spectra. These yield spectra contain the yield information about the electron degradation process and can be employed to calculate the yield for any inelastic event. The numerical yield spectra generated in this way are in turn represented analytically, which contains the information about all possible collisional events based on the input electron impact cross sections, resulting in the AYS. This yield spectrum can be used to calculate the steady state photoelectron flux. More details of the AYS approach and the method of photoelectron computation are given in several previous papers (Singhal & Haider 1984; Bhardwaj et al. 1990, 1996; Singhal & Bhardwaj 1991; Bhardwaj 1999, 2003; Bhardwaj & Michael 1999b; Haider & Bhardwaj 2005; Bhardwaj & Jain 2009, 2011; Raghuram & Bhardwaj 2011). The total inelastic electron impact cross sections for  $\text{H}_2\text{O}$  are taken from Jackman et al. (1977) and Seng & Linder (1976), and those for  $\text{CO}_2$  and  $\text{CO}$  are taken from Jackman et al. (1977). The electron impact cross sections for different dissociative ionization states of  $\text{H}_2\text{O}$  are taken from Itikawa & Mason (2005), for  $\text{CO}_2$  from Bhardwaj & Jain (2009), and for  $\text{CO}$  from McConkey et al. (2008). The volume excitation rates for different processes are calculated using steady state photoelectron flux and electron impact cross sections. The electron temperature required for ion-electron dissociative recombination reactions is taken from Körösmezey et al. (1987). The detailed description of coupled chemistry-transport model has been given in our earlier papers (Bhardwaj et al. 1995, 1996; Bhardwaj 1999; Bhardwaj & Haider 2002; Haider & Bhardwaj 2005; Bhardwaj & Raghuram 2011). Various reactions involved in the production and loss of metastable  $\text{O}(^1\text{S})$  and  $\text{O}(^1\text{D})$  atoms considered in our model are listed in Tables 1 and 2, respectively.

### 3. Dissociation of neutral species producing $\text{O}(^1\text{S})$ and $\text{O}(^1\text{D})$

#### 3.1. Photodissociation

##### 3.1.1. $\text{H}_2\text{O}$ and $\text{OH}$

The dissociation of  $\text{H}_2\text{O}$  molecule starts at wavelengths less than 2424 Å and the primary products are H and OH. But the pre-dissociation process mainly starts from 1860 Å (Watanabe & Zelikoff 1953). The threshold wavelength for the photoionization of  $\text{H}_2\text{O}$  is 984 Å. Hence, solar UV photons in the wavelength region 1860 to 984 Å can dissociate  $\text{H}_2\text{O}$  and produce different daughter products. The threshold wavelengths for the dissociation of  $\text{H}_2\text{O}$  resulting in the production of  $\text{O}(^1\text{S})$  and  $\text{O}(^1\text{D})$  are 1390 Å and 1770 Å, respectively. Till now, the photo-yield value for the production of  $\text{O}(^1\text{D})$  from  $\text{H}_2\text{O}$  have been measured in only two experiments. Slanger & Black (1982) measured the  $\text{O}(^1\text{D})$  yield in photodissociation of  $\text{H}_2\text{O}$  at 1216 Å, and found its value to be 10%. McNesby et al. (1962) reported a 25% yield for the production of  $\text{O}(^1\text{D})$  or  $\text{O}(^1\text{S})$  at 1236 Å from  $\text{H}_2\text{O}$ .

Huebner et al. (1992) calculated photo production rates for different excited species produced from  $\text{H}_2\text{O}$  using absorption and ionization cross sections compiled from different experimental measurements. In our model the cross sections for the production of  $\text{O}(^1\text{D})$  in photodissociation of  $\text{H}_2\text{O}$  are taken from Huebner et al. (1992), which were determined based on experiments of Slanger & Black (1982) and McNesby et al. (1962). Huebner et al. (1992) assumed that in the 1770 to 1300 Å wavelength region around 25% of  $\text{H}_2\text{O}$  molecules photodissociate into  $\text{H}_2$  and  $\text{O}(^1\text{D})$ , while between 1300 and 984 Å about 10% of  $\text{H}_2\text{O}$  dissociation produces  $\text{O}(^1\text{D})$  (cf. Fig. 4). Below 984 Å, Huebner et al. (1992) assumed that 33% of dissociation of  $\text{H}_2\text{O}$  leads to the formation of  $\text{O}(^1\text{D})$ . Festou (1981) discussed various dissociation channels for  $\text{H}_2\text{O}$  in the wavelength region less than 1860 Å. Solar photons in the wavelength region 1357 to 1860 Å dissociates around 72% of  $\text{H}_2\text{O}$  molecules into ground states of H and OH. But, according to Stief et al. (1975) approximately 1% of  $\text{H}_2\text{O}$  molecules are dissociated into  $\text{H}_2$  and  $\text{O}(^1\text{D})$  in this wavelength region. The calculated rates for the  $\text{O}(^1\text{D})$  production from photodisso-

ciative excitation of H<sub>2</sub>O by Huebner et al. (1992) are  $5.97 \times 10^{-7} \text{ s}^{-1}$  and  $1.48 \times 10^{-6} \text{ s}^{-1}$  for solar quiet and active conditions, respectively. Using the S2K solar EUV-UV flux on 1996 March 30 and cross sections from Huebner et al. (1992) (see Figure 4), our calculated value is  $8 \times 10^{-7} \text{ s}^{-1}$  (cf. Table 2), which is a factor of  $\sim 1.5$  higher than that of Huebner et al. (1992) for solar minimum condition at 1 AU. This difference in calculated values is mainly due to the higher (a factor of 1.24) value of solar flux at 1216 Å in S2K model than that used by Huebner et al. (1992) (cf. Figure 2).

No experimentally determined cross sections for the production of O(<sup>1</sup>S) in photodissociation of H<sub>2</sub>O are available. The solar flux at H Lyman- $\alpha$  (cf. Fig. 2) is more than an order of magnitude larger than the flux at wavelengths below 1390 Å, which is the threshold for the O(<sup>1</sup>S) production in dissociation of H<sub>2</sub>O. To account for the production of O(<sup>1</sup>S) in photodissociation of H<sub>2</sub>O, we assumed an yield of 0.5% at solar H Lyman- $\alpha$  (1216 Å). However, to assess the impact of this assumption on the green and red line emissions we varied the yield between 0 and 1%. The calculated photo-rate for the production of O(<sup>1</sup>S) from H<sub>2</sub>O is  $6.4 \times 10^{-8} \text{ s}^{-1}$  at 1 AU assuming 1% yield at 1216 Å (cf. Table 1).

The primary dissociative product of H<sub>2</sub>O is OH. The important destruction mechanisms of OH molecule are pre-dissociation through fluorescence process and direct photodissociation. The solar radiation shortward of 928 Å can ionize OH molecule. The threshold wavelengths for the production of O(<sup>1</sup>D) and O(<sup>1</sup>S) in photodissociation of OH are 1940 and 1477 Å, respectively. The dissociation channels of OH have been discussed by Budzien et al. (1994) and van Dishoeck & Dalgarno (1984). We have used the photo-rates given by Huebner et al. (1992) for the production of O(<sup>1</sup>D) and O(<sup>1</sup>S) from OH molecule whose values are  $6.4 \times 10^{-7}$  and  $6.7 \times 10^{-8} \text{ s}^{-1}$ , respectively. These rates are based on dissociation cross sections of van Dishoeck & Dalgarno (1984), which are consistent with the red line observation made by wide-field spectrometer (Morgenthaler et al. 2007).

### 3.1.2. CO<sub>2</sub>

The threshold wavelengths for dissociation of CO<sub>2</sub> molecule producing O(<sup>1</sup>D) and O(<sup>1</sup>S) are

1671 Å and 1286 Å, respectively. As noted by Huestis & Slanger (2006), the O(<sup>1</sup>D) yield in photodissociation of CO<sub>2</sub> has never been measured because of the problem of rapid quenching of this metastable state. However, experiment by Kedzierski et al. (1998) suggested that this dissociation channel can be studied in electron impact experiment using solid neon matrix as detector. Huebner et al. (1992) estimated the cross section for O(<sup>1</sup>D) production in photodissociative excitation of CO<sub>2</sub> (see Figure 4), and obtained photo-rate values of  $9.24 \times 10^{-7}$  and  $1.86 \times 10^{-6} \text{ s}^{-1}$  for solar minimum and maximum conditions, respectively. Using S2K solar flux on 1996 March 30 our calculated rate for O(<sup>1</sup>D) production in photodissociation of CO<sub>2</sub> is  $1.2 \times 10^{-6} \text{ s}^{-1}$  at 1 AU, which is higher than the solar minimum rate of Huebner et al. (1992) by a factor of 1.3. This variation is mainly due to the differences in the solar fluxes (cf. Figure 2) in the wavelength region 950 to 1100 Å where the photodissociative cross section for the production of O(<sup>1</sup>D) maximizes (cf. Figure 4).

Lawrence (1972) measured the O(<sup>1</sup>S) yield in photodissociative excitation of CO<sub>2</sub> from threshold (1286 Å) to 800 Å. The yield of Lawrence (1972) is different from that measured by Slanger et al. (1977) in the 1060 to 1175 Å region. However, the yield from both experimental measurements closely matches in the 1110–1140 Å wavelength region, where the yield is unity. In the experiment of Slanger et al. (1977), a dip in quantum yield is observed at 1089 Å. Huestis et al. (2010) reviewed the experimental results and suggested the yield for O(<sup>1</sup>S) in photodissociation of CO<sub>2</sub>. We calculated the cross section for the O(<sup>1</sup>S) production in photodissociative excitation of CO<sub>2</sub> (see Figure 4) by multiplying the yield recommended by Huestis et al. (2010) with total absorption cross section of CO<sub>2</sub> (see Figure 3). Using this cross section and S2K solar flux, the rate for O(<sup>1</sup>S) production is  $7.2 \times 10^{-7} \text{ s}^{-1}$  at 1 AU.

### 3.1.3. CO

The threshold wavelength for the dissociation of CO molecule into neutral products in the ground state is 1117.8 Å and in the metastable O(<sup>1</sup>D) and C(<sup>1</sup>D) is 863.4 Å. Among the O-bearing species discussed in this paper, CO has the highest dissociation energy of 11.1 eV, while its ionization potential is 14 eV. Huebner et al. (1992) calcu-

lated cross sections for the photodissociative excitation of CO producing O(<sup>1</sup>D) using branching ratios from McElroy & McConnell (1971) (cf. Fig. 4). Rates for the production of O(<sup>1</sup>D) from CO molecule calculated by Huebner et al. (1992) are  $3.47 \times 10^{-8}$  and  $7.87 \times 10^{-8} \text{ s}^{-1}$  for solar minimum and maximum conditions, respectively. Using the cross section of Huebner et al. (1992) and S2K model solar flux, our calculated rate for the O(<sup>1</sup>D) production from CO is  $5.1 \times 10^{-8} \text{ s}^{-1}$  at 1 AU, which is 1.5 times higher than the solar minimum rate of Huebner et al. (1992). This difference in the calculated value is due to variation in the solar fluxes used in the two studies in wavelength region 600 to 800 Å (cf. Figure 2).

We did not find any reports on the cross section for the production of O(<sup>1</sup>S) in photodissociation of the CO molecule. According to Huebner & Carpenter (1979) the rate for this reaction can not be more than  $4 \times 10^{-8} \text{ s}^{-1}$ . We have used this value in our model calculations. This process can be an important source of O(<sup>1</sup>S) since the comet Hyakutake has a higher CO abundance (~20%). Using this photorate and CO abundance, we will show that this reaction alone can contribute up to a maximum of 30% to the total O(<sup>1</sup>S) production.

### 3.2. Electron impact dissociation

In our literature survey we could not find any reported cross section for the production of O(<sup>1</sup>D) due to electron impact dissociation of H<sub>2</sub>O. Jackman et al. (1977) have assembled the experimental and theoretical cross sections for electron impact on important atmospheric gases in a workable analytical form. The cross sections for electron impact on atomic oxygen given by Jackman et al. (1977) have been used to estimate emissions which leave the O atom in the metastable (<sup>1</sup>D) state. The obtained ratios of 85% in ground and 15% in metastable state are used for the atomic states of C and O produced in electron impact dissociation of H<sub>2</sub>O, CO<sub>2</sub>, and CO. It may be noted that the ground state to metastable state production ratio of 89:11 is observed for atomic carbon and atomic oxygen produced from photodissociation of CO (Singh et al. 1991). However, as shown later, the contributions of these electron impact processes to the total production of O(<sup>1</sup>D) are very small (<5%).

Kedzierski et al. (1998) measured the cross section for electron impact dissociative excitation of H<sub>2</sub>O producing O(<sup>1</sup>S), with overall uncertainty of 30%. LeClair & McConkey (1994) measured cross section for the production of O(<sup>1</sup>S) in dissociation of CO<sub>2</sub> by electron impact; they claimed an uncertainty of 12% in their experimental cross section measurements. The cross section for fragmentation of CO into metastable O(<sup>1</sup>S) atom by electron impact is measured by LeClair et al. (1994). These electron impact cross sections are also recommended by McConkey et al. (2008), and are used in our model for calculating the production rate of O(<sup>1</sup>S) from H<sub>2</sub>O, CO<sub>2</sub>, and CO.

Since the <sup>1</sup>D and <sup>1</sup>S are metastable states, the direct excitation of atomic oxygen by solar radiation is not an effective excitation mechanism. However the electron impact excitation of atomic oxygen can populate these excited metastable states, which is a major source of airglow emissions in the upper atmospheres of Venus, Earth, and Mars. We calculated the excitation rates for these processes using electron impact cross sections from Jackman et al. (1977). In calculating the photoelectron impact ionization rates of metastable oxygen states, we calculated the cross sections by changing the threshold energy parameter for ionization of neutral atomic oxygen in the analytical expression given by Jackman et al. (1977). The above mentioned electron impact cross sections for the production of O(<sup>1</sup>S) from H<sub>2</sub>O, CO<sub>2</sub>, CO, and O, used in the current model, are presented in Figure 5 along with the calculated photoelectron flux energy spectrum at cometocentric distance of 1000 km.

### 3.3. Dissociative recombination

The total dissociative recombination rate for H<sub>2</sub>O<sup>+</sup> reported by Rosen et al. (2000) is  $4.3 \times 10^{-7} \text{ cm}^{-3} \text{ s}^{-1}$  at 300 K. The channels of dissociative recombination have also been studied by this group. It was found that the dissociation process is dominated by three-body breakup (H + H + O) that occurs with a branching ratio of 0.71, while the fraction of two-body breakup (O + H<sub>2</sub>) is 0.09, and the branching ratio for the formation of OH + H is 0.2. The maximum kinetic energy of the dissociative products forming atomic oxygen produced in ground state are 3.1 eV and 7.6 eV for the three- and two-body dissociation, re-

spectively. Since the excitation energy required for the formation of metastable  $O(^1S)$  is 4.19 eV, the three-body dissociation can not produce oxygen atoms in  $^1S$  state. However, the  $O(^1D)$  atom can be produced in both, the three-body and the two-body, breakup dissociation processes. To incorporate the contribution of  $H_2O^+$  dissociative recombination in the production of  $O(^1D)$  and  $O(^1S)$ , we assumed that 50% of branching fraction of the total recombination in three-body and two-body breakups lead to the formation of  $O(^1D)$  and  $O(^1S)$  atoms, respectively. For dissociative recombination of  $CO_2^+$ ,  $CO^+$  and  $OH^+$  ions we assumed that the recombination rates are same for the production of both  $O(^1D)$  and  $O(^1S)$ . We will show that these assumptions affects the calculated  $O(^1S)$  and  $O(^1D)$  densities only at larger ( $\geq 10^4$  km) cometocentric distances, but not in the inner coma. Tables 1 and 2 list the rates, along with the source reference, for these recombination reactions.

## 4. Results and discussion

### 4.1. Production and loss of $O(^1S)$ atom

The calculated  $O(^1S)$  production rate profiles for different processes in comet C/1996 B2 Hyakutake are presented in Figure 6. These calculations are made under the assumption of 0.5% yield of  $O(^1S)$  from  $H_2O$  at 1216 Å solar H Lyman- $\alpha$  line and 1%  $CO_2$  relative abundance. The major production source of  $O(^1S)$  is the photodissociative excitation of  $H_2O$  throughout the cometary coma. However, very close to the nucleus, the photodissociative excitation of  $CO_2$  is also an equally important process for the  $O(^1S)$  production. Above 100 km, the photodissociative excitation of  $CO_2$  and  $CO$  makes an equal contribution in the production of  $O(^1S)$ . Since the cross section for electron impact dissociative excitation of  $H_2O$ ,  $CO_2$ , and  $CO$  are small (see Figure 5), the contributions from electron impact dissociation to  $O(^1S)$  production are smaller by an order of magnitude or more than that due to photodissociative excitation. At larger cometocentric distances ( $>2 \times 10^3$  km), the dissociative recombination of  $H_2O^+$  ion is a significant production mechanism for  $O(^1S)$ , whose contribution is higher than those from photodissociative excitation of  $CO_2$  and  $CO$ . The dissociative recombination of other ions do not make

any significant contribution to the production of  $O(^1S)$ .

In the inner coma, the calculated production rates of  $O(^1S)$  via photodissociative excitation is  $CO_2$  at various wavelengths are presented in Figure 7. The major production of  $O(^1S)$  occurs in the wavelength region 955–1165 Å where the average cross section is  $\sim 2 \times 10^{-17}$   $cm^{-2}$  (cf. Fig. 4) and the average solar flux is  $\sim 1 \times 10^9$  photons  $cm^{-2} s^{-1}$  (cf. Fig. 2). The calculated loss rate profiles of  $O(^1S)$  for major processes are presented in Figure 8. Close to the nucleus ( $<50$  km), quenching by  $H_2O$  is the main loss mechanism for metastable  $O(^1S)$ . Above 100 km, the radiative decay of  $O(^1S)$  becomes the dominant loss process. The contributions from other loss processes are orders of magnitude smaller and hence are not shown in Figure 8.

### 4.2. Production and loss of $O(^1D)$ atom

The production rates as a function of cometocentric distance for various excitation mechanisms of the  $O(^1D)$  are shown in Figure 9. The major source of  $O(^1D)$  production in the inner coma is photodissociation of  $H_2O$ . The wavelength dependent production rates of  $O(^1D)$  from  $H_2O$  are presented in Figure 10. The  $O(^1D)$  production in photodissociation of  $H_2O$  is governed by solar radiation at H Lyman- $\alpha$  (1216 Å) wavelength. However, very close to the nucleus, the production of  $O(^1D)$  is largely due to photons in the wavelength region 1165–1375 Å. Since the average absorption cross section of  $H_2O$  decreases in this wavelength region by an order of magnitude, the optical depth at wavelengths greater than 1165 Å is quite small (see Figure 3). Hence, these photons are able to travel deeper into the coma unattenuated, thereby reaching close to the nucleus where they dissociate  $H_2O$  producing  $O(^1D)$ . Thus, at the surface of cometary nucleus the production of  $O(^1D)$  is controlled by the solar radiation in this wavelength band. In high production rate comets, the production of  $O(^1D)$  near nucleus would be governed by solar photons in this wavelength region. The production of  $O(^1D)$  from  $H_2O$  by solar photons from other wavelength regions is smaller by more than an order of magnitude.

After photodissociative excitation of  $H_2O$ , the next significant  $O(^1D)$  production process at radial distances below 50 km is the photodissociative



excitation of CO<sub>2</sub>. Above 50 km to about 1000 km, the radiative decay of O(<sup>1</sup>S), and at radial distances above 1000 km the dissociative recombination of H<sub>2</sub>O<sup>+</sup>, are the next potential sources of the O(<sup>1</sup>D) (see Figure 9). The calculated wavelength dependent production rates of O(<sup>1</sup>D) for photodissociation of CO<sub>2</sub> are shown in Figure 11. Solar radiation in the wavelength region 1165–955 Å dominates the O(<sup>1</sup>D) production. Since the cross section for the production of O(<sup>1</sup>D) due to photodissociation of CO<sub>2</sub> is more than an order of magnitude higher in this wavelength region compared to cross section at other wavelengths (see Figure 4), the solar radiation in this wavelength band mainly controls the formation of O(<sup>1</sup>D) from CO<sub>2</sub>. Other potential contributions are made by solar photons in the wavelength band 1585–1375 Å at distances <50 km, and 955–745 Å at radial distances >100 km. Since the CO<sub>2</sub> absorption cross section around 1216 Å is smaller by more than two orders of magnitude compared to its maximum value, the solar radiation at H Ly-α is not an efficient source of O(<sup>1</sup>D) atoms.

Zipf (1969) measured the total rate coefficient for the quenching of O(<sup>1</sup>S) by H<sub>2</sub>O as  $3 \times 10^{-10}$  cm<sup>3</sup> s<sup>-1</sup>. The primary channel in quenching mechanism is the production of two OH atoms. The production of O(<sup>1</sup>D) is also a possible channel whose rate coefficient is not reported in the literature. Hence, we assumed that 1% of total rate coefficient can lead to the formation of O(<sup>1</sup>D) in this quenching mechanism. However, this assumption has no implications on the O(<sup>1</sup>D) production since the total contribution due to O(<sup>1</sup>S) is about three orders of magnitude smaller than the major production process of O(<sup>1</sup>D).

The calculated loss rate profiles of O(<sup>1</sup>D) are presented in Figure 12. Below 1000 km, the O(<sup>1</sup>D) can be quenched by various cometary species. The quenching by H<sub>2</sub>O is the major loss mechanism for O(<sup>1</sup>D) below 500 km. Above  $2 \times 10^3$  km radiative decay is the dominant loss process for O(<sup>1</sup>D).

#### 4.3. Calculation of green and red-doublet emission intensity

Using the calculated production and loss rates due to various processes mentioned above, and assuming photochemical equilibrium, we computed the number density of O(<sup>1</sup>S) and O(<sup>1</sup>D) metastable atoms. The calculated number densi-

ties are presented in Figure 13. The O(<sup>1</sup>D) density profile shows a broad peak around 200–600 km. But, in the case of O(<sup>1</sup>S), the density peaks at much lower radial distances of ~60 km. The number densities of O(<sup>1</sup>D) and O(<sup>1</sup>S) are converted into emission rate profiles for the red-doublet and green line emissions, respectively, by multiplying with Einstein transition probabilities as

$$\begin{aligned} V_{(6300+6364)}(r) &= A_{(6300+6364)} \times [O^1D(r)] \\ &= A_{(6300+6364)} \frac{\sum_{i=1}^k P_i(r)}{\sum_{i=1}^k L_i(r) + A(^1D)} \end{aligned} \quad (7)$$

and

$$\begin{aligned} V_{(5577)}(r) &= A_{(5577)} \times [O^1S(r)] \\ &= A_{(5577)} \frac{\sum_{i=1}^k P_i(r)}{\sum_{i=1}^k L_i(r) + A(^1S)} \end{aligned} \quad (8)$$

Where  $[O^1S(r)]$  and  $[O^1D(r)]$  are the calculated number density for the corresponding production rates  $P_i(r)$  and loss frequencies  $L_i(r)$  for O(<sup>1</sup>S) and O(<sup>1</sup>D), respectively.  $A(^1D)$  and  $A(^1S)$  are the total Einstein spontaneous emission coefficients for red-doublet and green line emissions. Using the emission rate profiles, the line of sight intensity of green and red-doublet emissions along the projected distance  $z$  is calculated as

$$I(z) = 2 \int_z^R V_{(5577, 6300+6364)}(s) ds \quad (9)$$

where  $s$  is the abscissa along the line of sight, and  $V_{(5577, 6300+6364)}(s)$  is the emission rate for the green or red-doublet emission. The maximum limit of integration  $R$  is taken as  $10^5$  km. The calculated brightness profiles of 5577 and 6300 Å emissions are presented in Figure 14. These brightness profiles are then averaged over the projected area corresponding to the slit dimension  $1.2'' \times 8.2''$  centred on the nucleus of comet C/1996 B2 Hyakutake for the observation on 30 March 1986 (Cochran 2008). The G/R ratio averaged over the slit is also calculated.

#### 4.4. Model results

Morrison et al. (1997) observed the green and red-doublet emissions on comet C/1996 B2 Hyakutake in the high resolution optical spectra obtained on 1996 March 23 and 27 and found the G/R ratio

in the range 0.12–0.16. Cochran (2008) observed the 5577 and 6300 Å line emissions on this comet on 1996 March 9 and 30, with the G/R ratio as 0.09 for 9 March observation. We calculated the G/R ratio by varying the yield for O(<sup>1</sup>S) production in photodissociation of H<sub>2</sub>O at 1216 Å (henceforth refer to as O(<sup>1</sup>S) yield). Since CO<sub>2</sub> is not observed in this comet, we assumed that a minimum 1% CO<sub>2</sub> is present in the coma. However, we also carried out calculations for 0%, 3% and 5% CO<sub>2</sub> abundances in the comet. We calculated the contributions of different production processes in the formation of O(<sup>1</sup>S) and O(<sup>1</sup>D) at three different projected distances of 10<sup>2</sup>, 10<sup>3</sup>, and 10<sup>4</sup> km from the nucleus for the above mentioned CO<sub>2</sub> abundances and the O(<sup>1</sup>S) yield values varying from 0% to 1%. These calculations are presented in Table 3. The percentage contribution of major production processes in the projected field of view for the green and red-doublet emissions are also calculated. The G/R ratio is calculated after averaging the intensity over the projected area 165 × 1129 km which corresponds to the dimension of slit used in the observation made by Cochran (2008) on 1996 March 30. These calculated values are presented in Table 4.

Taking 1% CO<sub>2</sub> abundance and 0% O(<sup>1</sup>S) yield, the calculated percentage contributions of major production processes of O(<sup>1</sup>S) and O(<sup>1</sup>D) atoms are presented in Table 3. Around 60 to 90% of the O(<sup>1</sup>D) is produced from photodissociation of H<sub>2</sub>O. Contributions of photodissociative excitation of CO<sub>2</sub> and CO in the production of O(<sup>1</sup>S) and O(<sup>1</sup>D) are 15 to 40% and 1%, respectively. Around 10<sup>4</sup> km projected distance, the photodissociative excitation of OH (~20%) and the dissociative recombination of H<sub>2</sub>O<sup>+</sup> (~30%) are also significant production processes for O(<sup>1</sup>S) atoms. But, the contributions from these processes in O(<sup>1</sup>D) production is around 10% only.

For CO<sub>2</sub> abundance of 1% and O(<sup>1</sup>S) yield of 0.2%, the calculations presented in Table 3 show that the photodissociation of H<sub>2</sub>O contribute around 20 to 40% in the production of O(<sup>1</sup>S) and 60 to 90% in the production of O(<sup>1</sup>D) atom. The next major source of O(<sup>1</sup>S) production is the photodissociation of CO<sub>2</sub> and CO with each contributing ~10 to 25%. The relative contributions from photodissociation of parent species H<sub>2</sub>O, CO<sub>2</sub>, and CO to O(<sup>1</sup>S) and O(<sup>1</sup>D) production decreases with

increase in projected distance from the nucleus. At 10<sup>4</sup> km projected distance, the photodissociation of OH contribute 15% and 8% to the production of O(<sup>1</sup>S) and O(<sup>1</sup>D) atoms, respectively. Above 1000 km projected distance, the contribution of H<sub>2</sub>O<sup>+</sup> dissociative recombination to O(<sup>1</sup>S) production is around 20%. The production of O(<sup>1</sup>D) atom is mainly via photodissociation of H<sub>2</sub>O, but around 10<sup>4</sup> km the dissociative recombination of H<sub>2</sub>O<sup>+</sup> ion is also a significant production process contributing around 12%. At 10<sup>4</sup> km, dissociative recombination of OH<sup>+</sup> also contribute around 10% to the total O(<sup>1</sup>D) production, which is not shown in Table 3, and this value is independent of O(<sup>1</sup>S) yield or CO<sub>2</sub> abundance. Radiative decay of O(<sup>1</sup>S) is a minor (≤5%) production process in the formation of O(<sup>1</sup>D).

We also calculated the relative contributions of different processes in the formation of green and red line emissions in the slit projected field of view, which are presented in Table 4. For the above case, the photodissociation of H<sub>2</sub>O contribute around 35%, while the photodissociation of CO<sub>2</sub> and CO contribute 23% and 22%, respectively, to the production of green line emission. The contribution of dissociative recombination of H<sub>2</sub>O<sup>+</sup> ions is around 10%. The major production process of red lines is photodissociation of H<sub>2</sub>O (90%); the dissociative recombination of H<sub>2</sub>O<sup>+</sup> and radiative decay of O(<sup>1</sup>S) atom are minor (≤5%) production processes. With the O(<sup>1</sup>S) yield of 0.2% and 1% CO<sub>2</sub> abundance, the slit-averaged G/R ratio is found to be 0.11.

When the O(<sup>1</sup>S) yield is increased to 0.5% with 1% CO<sub>2</sub> abundance (see Table 3), the contribution from photodissociative excitation of H<sub>2</sub>O to the O(<sup>1</sup>S) production is increased, with value varying from 35 to 60%, while the contribution to O(<sup>1</sup>D) production is not changed. In this case, the contribution from photodissociation of CO<sub>2</sub> and CO to the O(<sup>1</sup>S) production is reduced (values between 10 to 15%). The contributions from other processes are not changed significantly. Table 4 shows that in this case around 60% of green line in the slit projected field of view is produced via photodissociation of H<sub>2</sub>O, while the contributions from photodissociation of CO<sub>2</sub> and CO are around 15% each. The main (90%) production of red-doublet emission is through photodissociation of H<sub>2</sub>O. The slit-averaged G/R ratio is 0.17.

On further increasing the  $O(^1S)$  yield to 1% with  $CO_2$  abundances of 1%, the contribution of photodissociation of  $H_2O$  to  $O(^1S)$  atom production is further increased (values between 50 to 75%) while the contribution from photodissociation of  $CO_2$  and  $CO$  is decreased to around 10% each (cf. Table 3). The contributions from other processes are not affected compared to the previous case. As seen from Table 4, in this case the contribution of photodissociation of  $H_2O$  to green line is around 75% in the slit projected field of view, while contributions from photodissociation of  $CO_2$  and  $CO$  are decreased to 10% each. The calculated G/R ratio is 0.27 (Table 4).

We also evaluated the effect of  $CO_2$  on the red-doublet and green line emissions by varying its abundance to 0%, 3% and 5%. The calculated percentage contribution of major processes along the projected distances and in the slit projected field of view are presented in Tables 3 and 4, respectively. In the absence of  $CO_2$ , the contributions from  $H_2O$ ,  $H_2O^+$  and  $CO$  in  $O(^1S)$  production are increased by  $\sim 10\%$  (cf. Tables 3 and 4). Taking 0%  $O(^1S)$  yield and by increasing  $CO_2$  relative abundance from 1 to 3%, the percentage contributions for  $O(^1S)$  from photodissociative excitation of  $CO_2$  ( $CO$ ) is increased (decreased) by 50%. The contribution from  $H_2O$  to  $O(^1D)$  production is not changed.

The calculations presented in Tables 3 and 4 depict that the contributions of various processes are significant in the production  $O(^1S)$  atom, whereas photodissociative excitation of  $H_2O$  is the main production process for  $O(^1D)$  atom. Since comet C/1996 B2 Hyakutake is rich in  $CO$  (abundance  $\sim 22\%$ ) compared to other comets, the contribution from  $CO$  photodissociation to  $O(^1S)$  production is significant (10–25%). In the case of a comet having  $CO$  abundance less than 20%, the major production source of metastable  $O(^1S)$  atom would be photodissociation of  $H_2O$  and  $CO_2$ .

#### 4.5. Comparison with observations

In 1996 March, the green and red-doublet emissions were observed in comet C/1996 B2 Hyakutake from two ground-based observatories (Morrison et al. 1997; Cochran 2008). Each observatory determined the G/R ratio using different slit size. Using a circular slit, the projected radial distance over the comet for Morrison et al. (1997) observa-

tion on March 23 and March 27 varied from 640 to 653 km, while for Cochran (2008) observation, using a rectangular slit, the projected area was  $480 \times 3720$  km on March 9 and  $165 \times 1129$  km on March 30. The clear detection of both green and red-doublet emissions and determination of the G/R ratio could be done for March 9 and March 23 observations only (Cochran 2008; Morrison et al. 1997). The observed G/R ratio was 0.09 and 0.12 to 0.16 for the observation on March 9 and March 23, respectively.

Making a very high resolution ( $R = 200,000$ ) observation of comet C/1996 B2 Hyakutake on 1996 March 30, Cochran (2008) obtained radial profiles of 5577 and 6300 Å lines. In Figure 14 we have compared the model calculated intensity profiles of 6300 and 5577 Å lines at different projected cometocentric distances with the observation of Cochran (2008). The calculated G/R ratio along projected distance is shown in Figure 15. The 6300 Å emission shows a flat profile upto  $\sim 500$  km, whereas the 5577 Å green line starts falling off beyond 100 km. This is because of the quenching of  $O(^1S)$  and  $O(^1D)$  by  $H_2O$  in the inner most coma (cf. Figures 8 and 12), thereby making both the production and loss mechanisms being controlled by  $H_2O$ . Above these distances, the emissions are mainly controlled by the radiative decay of  $^1S$  and  $^1D$  states of oxygen atoms.

Similar to the calculations presented in Tables 3 and 4, in Figures 14 and 15 we present the red and green line intensity profiles and the G/R ratios, respectively, for different contributions of  $O(^1S)$  yield and  $CO_2$  abundances. Since photodissociative excitation of  $H_2O$  is the main production process for  $O(^1D)$  atom, the red line intensity is almost independent of the variation in  $O(^1S)$  yield and  $CO_2$  abundance. In the case of 0%  $CO_2$  abundance, the best fit to the observed green line profile is obtained when the  $O(^1S)$  yield is  $\sim 0.5\%$  ( $\pm 0.1\%$ ), where the G/R ratio varied from 0.06 to 0.26 (cf. Figure 15) and the slit-averaged G/R ratio for March 30 observation is 0.15 (cf. Table 4). The shape of green line profile cannot be explained with 1% or 0%  $O(^1S)$  yield, while the case for 0.2%  $O(^1S)$  yield can be considered as somewhat consistent with the observation. For this case, the value of G/R ratio shown in Figure 15 is found to vary over a large range of 0.54 to 0.02.

When we consider 1%  $CO_2$  in the comet, the

best-fit green profile is obtained when the  $O(^1S)$  yield is  $\sim 0.2\%$ . The case for  $0.5\%$   $O(^1S)$  yield also provides the green line profile consistent with the observation. In both these cases the G/R ratio varies between 0.32 and 0.04 over the cometocentric projected distances of 10 to  $10^4$  km. The calculated  $5577 \text{ \AA}$  profiles for  $O(^1S)$  yield of 0% and 1% are inconsistent with the observed profile.

In Figure 14 we also show a calculated profile for a case when the  $CO_2$  abundance is 3% while the  $O(^1S)$  yield is 0% (i.e., no  $O(^1S)$  is produced in photodissociation of  $H_2O$ ). The calculated  $5577 \text{ \AA}$  green line profile shows a good fit to the observed profile: suggesting that even a small abundance of  $CO_2$  is enough to produce the required  $O(^1S)$ . This is because the  $CO_2$  is about an order of magnitude more efficient in producing  $O(^1S)$  atom than  $H_2O$  in the photodissociation process (see Table 1). However, since  $O(^1S)$  would definitely be produced in the photodissociation of  $H_2O$ , and that the  $CO_2$  would surely be present in comet (though in smaller abundance), the most consistent value for the  $O(^1S)$  yield would be around 0.5%. Assuming 5%  $CO_2$  and 0.5%  $O(^1S)$  yield, the calculated green line emission profile is inconsistent with the observation (cf. Figure 15). In this case, the calculated G/R ratio shown in Figure 15 is found to vary between 0.24 and 0.05.

From the above calculations it is clear that the slit projected area on to the comet also plays an important role in deciding the G/R ratio. This point can be better understood from Table 5 where the G/R ratio is presented for a projected square slit on the comet at different geocentric distances. It is clear from this table that for a given physical condition of a comet and at a given heliocentric distance, the observed G/R ratio for a given slit size can vary according to the geocentric distance of the comet. For example, for a  $O(^1S)$  yield of 0.2% (0.5%) and  $CO_2$  abundance of 1%, the G/R ratio can be 0.17 (0.26) if the comet is very close to the Earth (0.1 AU), whereas the G/R ratio can be 0.07 (0.1), 0.06 (0.08), or 0.06 (0.07), if the comet, at the time of observation, is at a larger distance of 0.5, 1, and 2 AU from the Earth, respectively. Further, a G/R ratio of  $\sim 0.1$  can be obtained even for the  $O(^1S)$  yield of 0%. This suggests that the value of 0.1 for the G/R ratio is in no way a definitive benchmark value to conclude that  $H_2O$  is the parent of atomic oxygen atom in the comet, since

smaller ( $\sim 5\%$  relative to  $H_2O$ ) amounts of  $CO_2$  and CO itself can produce enough  $O(^1S)$  compared to that from  $H_2O$ . This table also shows that for observations made around a geocentric distance of 1 AU, the G/R ratio would be generally closer to 0.1. The G/R ratio observed in different comets ranges from 0.02 to 0.3 (e.g., Cochran 2008; Capria et al. 2010).

Thus, we can conclude that the G/R ratio not only depends on the production and loss mechanisms of  $O(^1S)$  atom, but also depends on the nucleocentric slit projected area over the comet. Moreover, the  $CO_2$  plays an important role in the production of  $O(^1S)$ , and thus the green line emission, in comets. With the present model calculations and based on the literature survey of dissociation channels of  $H_2O$ , we suggest that the  $O(^1S)$  yield from photodissociation of  $H_2O$  cannot be more than 1% of the total absorption cross section of  $H_2O$  at solar Ly- $\alpha$  radiation. The best fit value of  $O(^1S)$  yield derived from Figure 14 for a smaller (1%)  $CO_2$  abundance in the comet C/1996 B2 Hyakutake is  $0.4 (\pm 0.1)\%$ . As per the Tables 1 and 2, this means that the ratio of rates of  $O(^1S)$  to  $O(^1D)$  production in the  $H_2O$  photodissociation should be  $0.03 (\pm 0.01)$ , which is much smaller than the value of 0.1 generally used in literature based on Festou & Feldman (1981). Further, if the source of red and green lines is  $CO_2$  (CO), the ratio of photorates for  $O(^1S)$  to  $O(^1D)$  would be around 0.6 (0.8) (see Tables 1 and 2).

To verify whether the  $O(^1S)$  yield of 0.5% (for the  $CO_2$  abundance of 1%) derived from Figure 14, based on the comparison between model and observed red and green line radial profiles in comet Hyakutake on 1996 March 30, is consistent with the G/R ratio observed on other days on this comet, we present in Table 6 the G/R ratio calculated for observations made on 1996 March 9, 23, 27, and 30, along with the observed value of G/R ratio from Morrison et al. (1997) and Cochran (2008). These calculations are made by taking the solar flux on the day of observation using Tobiska (2004) SOLAR2000 model and scaled according to the heliocentric distance of the comet on that date. The CO abundance is 22%, same as in all the calculations presented in the paper.

The calculated G/R ratio on March 9, when geocentric distance was 0.55 AU and  $H_2O$  production rate  $5 \times 10^{28} \text{ s}^{-1}$ , is 0.09 (see Table 6)

which is same as the observed ratio obtained by Cochran (2008). On March 23 and 27 the comet is closer to both Sun and Earth (geocentric distance  $\sim 0.1$  AU) and its  $\text{H}_2\text{O}$  production rate was 4 times higher than the value on March 9. The calculated G/R ratio on March 23 is 0.12, which is in agreement with the observed ratio obtained by Morrison et al. (1997).

## 5. Conclusions

The Green and red-doublet atomic oxygen emissions are observed in comet C/1996 B2 Hyakutake in 1996 March when it was passing quite close to the Earth ( $\Delta = 0.1$  to  $0.55$  AU). A coupled chemistry-emission model has been developed to study the production of green ( $5577 \text{ \AA}$ ) and red-doublet ( $6300$  and  $6364 \text{ \AA}$ ) emissions in comets. This model has been applied to comet Hyakutake and the results are compared with the observed radial profiles of  $5577$  and  $6300 \text{ \AA}$  line emissions and the green to red-doublet intensity ratio. The important results from the present model calculations can be summarized as following. It may be noted that some of these results enumerated below may vary for other comets having different gas production rate or heliocentric distance.

1. The photodissociation of  $\text{H}_2\text{O}$  is the dominant production process for the formation of  $\text{O}(^1\text{D})$  throughout the inner cometary coma. The solar H Ly- $\alpha$  ( $1216 \text{ \AA}$ ) flux mainly governs the production of  $\text{O}(^1\text{D})$  in the photodissociative excitation of  $\text{H}_2\text{O}$ , but near the nucleus solar radiation in the wavelength band  $1375\text{--}1165 \text{ \AA}$  can control the formation of  $\text{O}(^1\text{D})$  from  $\text{H}_2\text{O}$ .
2. Other than the photodissociation of  $\text{H}_2\text{O}$  molecule, above cometocentric distance of  $100 \text{ km}$  the radiative decay of  $\text{O}(^1\text{S})$  to  $\text{O}(^1\text{D})$  (via  $5577 \text{ \AA}$  line emission), while above  $1000 \text{ km}$  the dissociative recombination of  $\text{H}_2\text{O}^+$  ions, are also significant source mechanisms for the formation of  $\text{O}(^1\text{D})$  and  $\text{O}(^1\text{S})$  atoms.
3. The collisional quenching of  $\text{O}(^1\text{D})$  atoms by  $\text{H}_2\text{O}$  is significant up to radial distance of  $\sim 1000 \text{ km}$ ; above this distance the radiative decay is the main loss mechanism of  $\text{O}(^1\text{D})$

atoms. The collisional quenching of  $\text{O}(^1\text{D})$  by other neutral species is an order of magnitude smaller.

4. The photodissociation of  $\text{H}_2\text{O}$  is the major process for the production of  $\text{O}(^1\text{S})$  atoms, but near the nucleus the photodissociation of  $\text{CO}_2$  can be the dominant source. The solar H Ly- $\alpha$  ( $1216 \text{ \AA}$ ) flux controls the production of  $\text{O}(^1\text{S})$  via photodissociative excitation of  $\text{H}_2\text{O}$ .
5. At cometocentric distances of  $< 100 \text{ km}$ , the main loss process for  $\text{O}(^1\text{S})$  is quenching by  $\text{H}_2\text{O}$  molecule, while above  $100 \text{ km}$  the radiative decay is the dominant loss process.
6. Since the photoabsorption cross section of  $\text{CO}_2$  molecule is quite small at  $1216 \text{ \AA}$ , the contribution of  $\text{CO}_2$  in the production of  $\text{O}(^1\text{S})$  and  $\text{O}(^1\text{D})$  at the solar H Ly- $\alpha$  is insignificant.
7. Because the  $\text{CO}_2$  absorption cross section in the  $1165\text{--}955 \text{ \AA}$  wavelength range is higher by an order of magnitude compared to that at other wavelengths, the solar radiation in this wavelength region mainly controls the production of  $\text{O}(^1\text{D})$  and  $\text{O}(^1\text{S})$  in the photodissociative excitation of  $\text{CO}_2$ . Moreover, the  $\text{CO}_2$  absorption cross section in this band is also the largest compared to those of  $\text{H}_2\text{O}$  and  $\text{CO}$ .
8. The cross section for the photodissociation of  $\text{H}_2\text{O}$  producing  $\text{O}(^1\text{S})$  at the solar H Ly- $\alpha$  wavelength (with  $1\%$   $\text{O}(^1\text{S})$  yield) is smaller by more than two orders of magnitude than the cross section for the photodissociation of  $\text{CO}_2$  producing  $\text{O}(^1\text{S})$  in the wavelength region  $1165\text{--}955 \text{ \AA}$ . Though the solar flux at  $1216 \text{ \AA}$  is higher compared to that in the  $1165\text{--}955 \text{ \AA}$  wavelength region by two orders of magnitude, the larger value of  $\text{CO}_2$  cross section in this wavelength band enables  $\text{CO}_2$  to be an important source for the production of metastable  $\text{O}(^1\text{S})$  atom.
9. In the case of  $\text{CO}$ , the dissociation and ionization thresholds are close to each other. Hence, most of the solar radiation ionizes  $\text{CO}$  molecule rather than producing the  $\text{O}(^1\text{S})$  and  $\text{O}(^1\text{D})$  atoms.

10. Though the CO abundance is relatively high ( $\sim 22\%$ ) in comet C/1996 B2 Hyakutake, the contribution of CO photodissociation in the  $O(^1D)$  production is small ( $\sim 1\%$ ), while for the production of  $O(^1S)$  its contribution is 10 to 25%.
11. The photoelectron impact dissociative excitation of  $H_2O$ ,  $CO_2$ , and CO makes only a minor contribution ( $< 1\%$ ) in the formation of metastable  $O(^1S)$  and  $O(^1D)$  atoms in the inner coma.
12. The  $O(^1S)$  density peaks at shorter radial distances than the  $O(^1D)$  density. The peak value of  $O(^1S)$  density is found around 60 km from the nucleus, while for the  $O(^1D)$  a broad peak around 200-600 km is observed.
13. In a  $H_2O$ -dominated comet, the green line emission is mainly generated in the photodissociative excitation of  $H_2O$  with contribution of 40 to 60% (varying according to the radial distance) to the total intensity, while the photodissociation of  $CO_2$  is the next potential source contributing 10 to 40%.
14. For the red line emission the major source is photodissociative excitation of  $H_2O$ , with contribution varying from 60 to 90% depending on the radial distance from the nucleus.
15. The G/R ratio depends not only on the production and loss processes of the  $O(^1S)$  and  $O(^1D)$  atoms, but also on the size of observing slit and the geocentric distance of comet at the time of observation.
16. For a fixed slit size, the calculated value of the G/R ratio is found to vary between 0.03 and 0.5 depending on the geocentric distance of the comet. In the inner ( $< 300$  km) most part of the coma, the G/R ratio is always larger than 0.1, with values as high as 0.5. On the other hand, at cometocentric distances larger than 1000 km the G/R ratio is always less than 0.1.
17. The model calculated radial profiles of 6300 and 5577 Å lines are consistent with the observed profiles on comet C/1996 B2 Hyakutake for  $O(^1S)$  yield of 0.4 ( $\pm 0.1$ ) and  $CO_2$  abundances of 1%.

18. The model calculated G/R ratio on comet Hyakutake is in good agreement with the G/R ratio observed on two days in 1996 March by two observatories using different slit sizes.

### Acknowledgments

S. Raghuram was supported by the ISRO Senior Research Fellowship during the period of this work.

### REFERENCES

- Atkinson, R., Baulch, D. L., Cox, R. A., Hampson, Jr., R. F., Kerr, J. A., Rossi, M. J., & Troe, J. 1997, *J. Phys. Chem. Ref. Data*, 26, 1329
- Atkinson, R., & Welge, K. H. 1972, *J. Chem. Phys.*, 57, 3689
- Berrington, K. A., & Burke, P. G. 1981, *Planet. Space Sci.*, 29, 377
- Bhardwaj, A. 1999, *J. Geophys. Res.*, 104, 1929
- . 2003, *Geophys. Res. Lett.*, 30
- Bhardwaj, A., & Haider, S. A. 2002, *Adv. Space Res.*, 29, 745
- Bhardwaj, A., Haider, S. A., & Singhal, R. P. 1990, *Icarus*, 85, 216
- . 1995, *Adv. Space Res.*, 16 (2), 31
- . 1996, *Icarus*, 120, 412
- Bhardwaj, A., & Jain, S. K. 2009, *J. Geophys. Res.*, 114, 11309
- . 2011, *Icarus*, .
- Bhardwaj, A., & Michael, M. 1999a, *J. Geophys. Res.*, 104, 24713
- . 1999b, *Geophys. Res. Lett.*, 26, 393
- Bhardwaj, A., & Raghuram, S. 2011, *MNRAS*, 412, L25
- Bhardwaj, A., & Singhal, R. P. 1993, *J. Geophys. Res.*, 98, 9473
- Biver, N., et al. 1999, *AJ*, 118, 1850
- Mitchell, J. B. A 1990, *Phys. Rep.*, 186, 215

- Budzien, S. A., Festou, M. C., & Feldman, P. D. 1994, *Icarus*, 107, 164
- Capetanakis, F. P., Sondermann, F., Höser, S., & Stuhl, F. 1993, *J. Chem. Phys.*, 98, 7883
- Capria, M. T., Cremonese, G., Bhardwaj, A., & Sanctis, M. C. D. 2005, *A&A*, 442, 1121
- Capria, M. T., Cremonese, G., Bhardwaj, A., Sanctis, M. C. D., & Epifani, E. M. 2008, *A&A*, 479, 257
- Capria, M. T., Cremonese, G., & Sanctis, M. C. D. 2010, *A&A*
- Cochran, A. L. 2008, *Icarus*, 198, 181
- Cochran, A. L., & Cochran, W. D. 2001, *Icarus*, 154, 381
- Cochran, W. D. 1984, *Icarus*, 58, 440
- Combi, M. R., Brown, M. E., Feldman, P. D., Keller, H. U., Meier, R. R., & Smyth, W. H. 1998, *ApJ*, 494, 816
- Combi, M. R., Harris, W. M., & Smyth, W. H. 2004, *Gas dynamics and kinetics in the cometary coma: theory and observations*, ed. Festou, M. C., Keller, H. U., & Weaver, H. A., 523–552
- Combi, M. R., Mäkinen, J. T. T., Bertaux, J.-L., & Quemérais, E. 2005, *Icarus*, 177, 228
- Delsemme, A. H., & Combi, M. R. 1976, *ApJ*, 209, L149
- . 1979, *ApJ*, 228, 330
- Demore, W. B., et al. 1997, *Chemical Kinetics and photochemical data for use in stratospheric modeling*, Tech. Rep. Evaluation Number 12
- Feldman, P. D., Cochran, A. L., & Combi, M. R. 2004, *Spectroscopic investigations of fragment species in the coma*, ed. Festou, M. C., Keller, H. U., & Weaver, H. A., 425–447
- Festou, M. C. 1981, *A&A*, 96, 52
- Festou, M. C., & Feldman, P. D. 1981, *A&A*, 103, 154
- Fink, U., & Johnson, J. R. 1984, *AJ*, 89, 1565
- Furusho, R., Kawakita, H., Fuse, T., & Watanabe, J. 2006, *Adv. Space Res.*, 38, 1983
- Glinski, R. J., Ford, B. J., Harris, W. M., Anderson, C. M., & Morgenthaler, J. P. 2004, *ApJ*, 608, 601
- Gueberman, S. L. 1995, *J. Chem. Phys.*, 102, 22
- Haider, S. A., & Bhardwaj, A. 2005, *Icarus*, 177, 196
- Huebner, W. F., & Carpenter, C. W. 1979, *Los Alamos Report*, 8085
- Huebner, W. F., Keady, J. J., & Lyon, S. P. 1992, *Adv. Space Sci.*, 195, 1
- Huestis, D. L., & Slanger, T. G. 2006, in *BAAS*, Vol. 38, AAS/Division for Planetary Sciences Meeting Abstracts, 609
- Huestis, D. L., Slanger, T. G., Sharpee, B. D., & Fox, J. L. 2010, *Faraday Discussions*, 147, 307
- Itikawa, Y., & Mason, N. 2005, *J. Phys. Chem. Ref. Data*, 34, 1
- Jackman, C. H., Garvey, R. H., & Green, A. E. S. 1977, *J. Geophys. Res.*, 82, 5081
- Kedzierski, W., Derbyshire, J., Malone, C., & McConkey, J. W. 1998, *J. Phys. B Atomic Molecular Physics*, 31, 5361
- Körösmezey, A., et al. 1987, *J. Geophys. Res.*, 92, 7331
- Krauss, M., & Neumann, D. 1975, *Chem. Phys. Lett.*, 36, 372
- Lawrence, G. M. 1972, *J. Chem. Phys.*, 57, 5616
- LeClair, L. R., Brown, M. D., & McConkey, J. W. 1994, *Chem. Phys.*, 189, 769
- LeClair, L. R., & McConkey, J. W. 1994, *J. Phys. B Atomic Molecular Physics*, 27, 4039
- Link, R. 1982, *PhD thesis*, York University, CANADA
- Magee-Sauer, K., Scherb, F., Roesler, F. L., & Harlander, J. 1990, *Icarus*, 84, 154
- Manfroid, J., et al. 2007, *Icarus*, 187, 144

- McConkey, J. W., Malone, C. P., Johnson, P. V., Winstead, C., McKoy, V., & Kanik, I. 2008, *Phys. Rep.*, 466, 1
- McElroy, M. B., & McConnell, J. C. 1971, *J. Geophys. Res.*, 76, 6674
- McNesby, J. R., Tanaka, I., & Okabe, H. 1962, *J. Chem. Phys.*, 36, 605
- Morgenthaler, J. P., Harris, W. M., & Combi, M. R. 2007, *ApJ*, 657, 1162
- Morgenthaler, J. P., et al. 2001, *ApJ*, 563, 451
- Morrison, N. D., Knauth, D. C., Mulliss, C. L., & Lee, W. 1997, *PASP*, 109, 676
- Mumma, M. J., DiSanti, M. A., Russo, N. D., Fomenkova, M., Magee-Sauer, K., Kaminski, C. D., & Xie, D. X. 1996, *Science*, 272, 1310
- Raghuram, S., & Bhardwaj, A. 2011, *Planet. Space Sci.*, in press
- Rosen, S., et al. 2000, *Faraday Discuss.*, 407, 295
- Schmidt, H. U., Wegmann, R., Huebner, W. F., & Boice, D. C. 1988, *Comp. Phy. Comm.*, 49, 17
- Schultz, D., Li, G. S. H., Scherb, F., & Roesler, F. L. 1992, *Icarus*, 96, 190
- Seng, G., & Linder, F. 1976, *J. Phys. B Atomic Molecular Physics*, 9, 2539
- Singh, P. D., D'Ealmeida, A. A., & Huebner, W. F. 1991, *Icarus*, 90, 74
- Singhal, R. P., & Bhardwaj, A. 1991, *J. Geophys. Res.*, 96, 15963
- Singhal, R. P., & Haider, S. A. 1984, *J. Geophys. Res.*, 89, 6847
- Slanger, T. G., & Black, G. 1982, *J. Chem. Phys.*, 77, 2432
- Slanger, T. G., Sharpless, R. L., & Black, G. 1977, *J. Chem. Phys.*, 66, 5317
- Spinrad, H. 1982, *PASP*, 94, 1008
- Stief, L. J., Payne, W. A., & Klemm, R. B. 1975, *J. Chem. Phys.*, 62, 4000
- Storey, P. J., & Zeippen, C. J. 2000, *MNRAS*, 312, 813
- Tobiska, W. K. 2004, *Adv. Space Res.*, 34, 1736
- Tobiska, W. K., Woods, T., Eparvier, F., Viereck, R., Floyd, L., Bouwer, D., Rottman, G., & White, O. R. 2000, *J. Atmos. Solar-Terres. Phys.*, 62, 1233
- van Dishoeck, E. F., & Dalgarno, A. 1984, *ApJ*, 277, 576
- Watanabe, K., & Zelikoff, M. 1953, *J. Optical Soc. America (1917-1983)*, 43, 753
- Wiese, W. L., Fuhr, J. R., & Deters, T. M., eds. 1996, *Atomic Transition Probabilities of Carbon, Nitrogen, and Oxygen: A Critical Data Compilation (Am. Chem. Soc., Washington, D. C.)*
- Zhang, H. W., Zhao, G., & Hu, J. Y. 2001, *A&A*, 367, 1049
- Zipf, E. C. 1969, *Can. J. Chem.*, 47, 1863



TABLE 1  
REACTIONS FOR THE PRODUCTION AND LOSS OF O(<sup>1</sup>S).

Reaction	Rate (cm <sup>3</sup> s <sup>-1</sup> or s <sup>-1</sup> )	Reference
H <sub>2</sub> O + hν → O( <sup>1</sup> S) + H <sub>2</sub>	6.4 × 10 <sup>-8</sup> <sup>a</sup>	This work
OH + hν → O( <sup>1</sup> S) + H	6.7 × 10 <sup>-8</sup>	Huebner et al. (1992)
CO <sub>2</sub> + hν → O( <sup>1</sup> S) + CO	7.2 × 10 <sup>-7</sup>	This work
CO + hν → O( <sup>1</sup> S) + C	4.0 × 10 <sup>-8</sup>	Huebner & Carpenter (1979)
H <sub>2</sub> O + e <sub>ph</sub> → O( <sup>1</sup> S) + others	9.0 × 10 <sup>-10</sup>	This work
OH + e <sub>ph</sub> → O( <sup>1</sup> S) + others	2.2 × 10 <sup>-10</sup>	This work
CO <sub>2</sub> + e <sub>ph</sub> → O( <sup>1</sup> S) + others	4.4 × 10 <sup>-8</sup>	This work
CO + e <sub>ph</sub> → O( <sup>1</sup> S) + others	2.2 × 10 <sup>-10</sup>	This work
O + e <sub>ph</sub> → O( <sup>1</sup> S)	3.0 × 10 <sup>-8</sup>	This work
H <sub>2</sub> O <sup>+</sup> + e <sub>th</sub> → O( <sup>1</sup> S) + others	4.3 × 10 <sup>-7</sup> (300/T <sub>e</sub> ) <sup>0.5</sup> × 0.045 <sup>b</sup>	Rosen et al. (2000)
OH <sup>+</sup> + e <sub>th</sub> → O( <sup>1</sup> S) + others	6.3 × 10 <sup>-9</sup> × (300/T <sub>e</sub> ) <sup>0.5</sup>	Gueberman (1995)
CO <sub>2</sub> <sup>+</sup> + e <sub>th</sub> → O( <sup>1</sup> S) + others	2.9 × 10 <sup>-7</sup> × (300/T <sub>e</sub> ) <sup>0.5</sup>	Mitchell (1990)
CO <sup>+</sup> + e <sub>th</sub> → O( <sup>1</sup> S) + others	5.0 × 10 <sup>-8</sup> × (300/T <sub>e</sub> ) <sup>0.46</sup>	Mitchell (1990)
O( <sup>1</sup> S) + hν → O <sup>+</sup> + e	1.9 × 10 <sup>-7</sup>	Huebner et al. (1992)
O( <sup>1</sup> S) + e <sub>ph</sub> → O <sup>+</sup> + 2e	2.7 × 10 <sup>-7</sup>	This work
O( <sup>1</sup> S) → O( <sup>3</sup> P) + hν <sub>2972</sub>	0.075	Wiese et al. (1996)
O( <sup>1</sup> S) → O( <sup>1</sup> D) + hν <sub>5577</sub>	1.26	Wiese et al. (1996)
O( <sup>1</sup> S) + H <sub>2</sub> O → 2 OH	3 × 10 <sup>-10</sup>	Zipf (1969)
→ O( <sup>1</sup> D) + H <sub>2</sub> O	3 × 10 <sup>-10</sup> × 0.01 <sup>c</sup>	Zipf (1969)
O( <sup>1</sup> S) + CO <sub>2</sub> → O( <sup>3</sup> P) + CO <sub>2</sub>	3.1 × 10 <sup>-11</sup> exp(-1330/T)	Atkinson & Welge (1972)
→ O( <sup>1</sup> D) + CO <sub>2</sub>	2.0 × 10 <sup>-11</sup> exp(-1327/T)	Capetanakis et al. (1993)
O( <sup>1</sup> S) + CO → CO + O	3.21 × 10 <sup>-12</sup> exp(-1327/T)	Capetanakis et al. (1993)
→ O( <sup>1</sup> D) + CO	7.4 × 10 <sup>-14</sup> exp(-961/T)	Capetanakis et al. (1993)
O( <sup>1</sup> S) + e <sub>th</sub> → O( <sup>1</sup> D) + e	8.56 × 10 <sup>-9</sup>	Berrington & Burke (1981)
→ O( <sup>3</sup> P) + e	1.56 × 10 <sup>-9</sup> (T <sub>e</sub> /300) <sup>0.94</sup>	Berrington & Burke (1981)
O( <sup>1</sup> S) + O → 2 O( <sup>1</sup> D)	2.0 × 10 <sup>-14</sup>	Krauss & Neumann (1975)

<sup>a</sup>This rate is calculated assuming 1% yield for the production of O(<sup>1</sup>S) at 1216 Å wavelength.

<sup>b</sup>0.045 is the assumed branching ratio for the formation of O(<sup>1</sup>S) via dissociative recombination of H<sub>2</sub>O<sup>+</sup> ion.

<sup>c</sup>0.01 is the assumed yield for the formation of O(<sup>1</sup>D) via quenching of H<sub>2</sub>O

NOTE.—The photorates and photoelectron impact rates are at 1 AU on 1996 March 30; e<sub>ph</sub> = photoelectron, e<sub>th</sub> = thermal electron, hν = solar photon, T<sub>e</sub> = electron temperature, T = neutral temperature.

TABLE 2  
REACTIONS FOR THE PRODUCTION AND LOSS OF O(<sup>1</sup>D).

Reaction	Rate (cm <sup>3</sup> s <sup>-1</sup> or s <sup>-1</sup> )	Reference
H <sub>2</sub> O + hν → O( <sup>1</sup> D) + H <sub>2</sub>	8.0 × 10 <sup>-7</sup>	This work
OH + hν → O( <sup>1</sup> D) + H	6.4 × 10 <sup>-7</sup>	Huebner et al. (1992)
CO <sub>2</sub> + hν → O( <sup>1</sup> D) + CO	1.2 × 10 <sup>-6</sup>	This work
CO + hν → O( <sup>1</sup> D) + C	5.1 × 10 <sup>-8</sup>	This work
O( <sup>1</sup> S) → O( <sup>1</sup> D) + hν <sub>557nm</sub>	1.26	Wiese et al. (1996)
H <sub>2</sub> O + e <sub>ph</sub> → O( <sup>1</sup> D) + H <sub>2</sub> + e	2.1 × 10 <sup>-10</sup>	This work
OH + e <sub>ph</sub> → O( <sup>1</sup> D) + H + e	7 × 10 <sup>-11</sup>	This work
CO <sub>2</sub> + e <sub>ph</sub> → O( <sup>1</sup> D) + CO + e	8.5 × 10 <sup>-9</sup>	This work
CO + e <sub>ph</sub> → O( <sup>1</sup> D) + C( <sup>1</sup> D) + e	7 × 10 <sup>-11</sup>	This work
O + e <sub>ph</sub> → O( <sup>1</sup> D)	3.7 × 10 <sup>-7</sup>	This work
H <sub>2</sub> O <sup>+</sup> + e <sub>th</sub> → O( <sup>1</sup> D) + H <sub>2</sub>	4.3 × 10 <sup>-7</sup> (300/T <sub>e</sub> ) <sup>0.5</sup> × 0.35 <sup>a</sup>	Rosen et al. (2000)
OH <sup>+</sup> + e <sub>th</sub> → O( <sup>1</sup> D) + H	6.3 × 10 <sup>-9</sup> × (300/T <sub>e</sub> ) <sup>0.48</sup>	Gueberman (1995)
CO <sub>2</sub> <sup>+</sup> + e <sub>th</sub> → O( <sup>1</sup> D) + CO	2.9 × 10 <sup>-7</sup> (300/T <sub>e</sub> ) <sup>0.5</sup>	Mitchell (1990)
CO <sup>+</sup> + e <sub>th</sub> → O( <sup>1</sup> D) + C( <sup>1</sup> D)	5 × 10 <sup>-8</sup> (300/T <sub>e</sub> ) <sup>0.46</sup>	Mitchell (1990)
O( <sup>1</sup> S) + e <sub>th</sub> → O( <sup>1</sup> D) + e	1.5 × 10 <sup>-10</sup> (T <sub>e</sub> /300) <sup>0.94</sup>	Berrington & Burke (1981)
O( <sup>1</sup> S) + H <sub>2</sub> O → O( <sup>1</sup> D) + H <sub>2</sub> O	3 × 10 <sup>-10</sup> × 0.01 <sup>b</sup>	Zipf (1969)
O( <sup>1</sup> S) + CO <sub>2</sub> → O( <sup>1</sup> D) + CO <sub>2</sub>	2.0 × 10 <sup>-11</sup> exp(-1327/T)	Capetanakis et al. (1993)
O( <sup>1</sup> S) + CO → O( <sup>1</sup> D) + CO	7.4 × 10 <sup>-14</sup> exp(-961/T)	Capetanakis et al. (1993)
O( <sup>1</sup> D) + hν → O <sup>+</sup> + e	1.82 × 10 <sup>-7</sup>	Huebner et al. (1992)
O( <sup>1</sup> D) → O( <sup>3</sup> P) + hν <sub>6300</sub>	6.44 × 10 <sup>-3</sup>	Storey & Zeippen (2000)
O( <sup>1</sup> D) → O( <sup>3</sup> P) + hν <sub>6364</sub>	2.15 × 10 <sup>-3</sup>	Storey & Zeippen (2000)
O( <sup>1</sup> D) + e <sub>ph</sub> → O <sup>+</sup> + 2e	1.75 × 10 <sup>-7</sup>	This work
O( <sup>1</sup> D) + e <sub>th</sub> → O( <sup>3</sup> P) + e	8.1 × 10 <sup>-10</sup> (T <sub>e</sub> /300) <sup>0.5</sup>	Link (1982)
O( <sup>1</sup> D) + H <sub>2</sub> O → OH + OH	2.1 × 10 <sup>-10</sup>	Atkinson et al. (1997)
→ O( <sup>3</sup> P) + H <sub>2</sub> O	9.0 × 10 <sup>-12</sup>	Atkinson et al. (1997)
→ H <sub>2</sub> + O <sub>2</sub>	2.2 × 10 <sup>-12</sup>	Atkinson et al. (1997)
O( <sup>1</sup> D) + CO <sub>2</sub> → O + CO <sub>2</sub>	7.4 × 10 <sup>-11</sup> exp(-120/T)	Atkinson et al. (1997)
→ CO + O <sub>2</sub>	2.0 × 10 <sup>-10</sup>	Atkinson et al. (1997)
O( <sup>1</sup> D) + CO → O + CO	5.5 × 10 <sup>-10</sup> exp(-625/T)	Schmidt et al. (1988)
→ CO <sub>2</sub>	8.0 × 10 <sup>-11</sup>	Demore et al. (1997)

<sup>a</sup>0.35 is the assumed branching ratio for the formation of O(<sup>1</sup>D) via dissociative recombination of H<sub>2</sub>O<sup>+</sup> ion.

<sup>b</sup>0.01 is the assumed branching ratio for the formation of O(<sup>1</sup>D) via quenching of H<sub>2</sub>O.

NOTE.—The photorates and photoelectron impact rates are at 1 AU on 1996 March 30, e<sub>ph</sub> = photoelectron, e<sub>th</sub> = thermal electron, hν = solar photon, T<sub>e</sub> = electron temperature, T = neutral temperature.



TABLE 4  
 CALCULATED PERCENTAGE CONTRIBUTION FOR THE MAJOR PRODUCTION PROCESSES OF THE GREEN  
 (RED-DOUBLET) EMISSION IN THE SLIT PROJECTED FIELD OF VIEW ON COMET C/1996 B2 HYAKUTAKE.

O( <sup>1</sup> S) Yield (%)	hν + H <sub>2</sub> O	hν + OH	hν + CO <sub>2</sub>	e <sup>-</sup> + H <sub>2</sub> O <sup>+</sup>	O( <sup>1</sup> S) → O( <sup>1</sup> D)	hν + CO	G/R ratio <sup>b</sup>
<b>1% CO<sub>2</sub></b>							
0.0	0 [91] <sup>a</sup>	2 [0.5]	36 [1]	13 [3]	[1]	35 [1]	0.07
0.2	36 [91]	1 [0.5]	23 [1]	8 [3]	[3]	22 [1]	0.11
0.5	59 [89]	1 [0.5]	14 [1]	5 [3]	[4]	14 [1]	0.17
1.0	76 [87]	0.5 [0.5]	10 [1]	0.5 [3]	[6]	10 [1]	0.27
<b>0% CO<sub>2</sub></b>							
0.0	0 [94]	4 [0.5]	0 [0]	21 [3]	[1]	59 [1]	0.04
0.2	49 [93]	2 [0.5]	0 [0]	11 [3]	[2]	30 [1]	0.08
0.5	70 [91]	1 [0.5]	0 [0]	6 [3]	[4]	17 [1]	0.15
1.0	82 [89]	0.5 [0.5]	0 [0]	3 [3]	[6]	10 [1]	0.25
<b>3% CO<sub>2</sub></b>							
0.0	0 [87]	1 [0.5]	60 [4]	7 [3]	[3]	20 [1]	0.13
<b>5% CO<sub>2</sub></b>							
0.0	35 [82]	0.5 [0.5]	45 [6]	3 [3]	[7]	7 [1]	0.27

<sup>a</sup>The values in square brackets are the calculated percentage contribution for the red-doublet emission.

<sup>b</sup>The calculated values are averaged over the projected area of 165 × 1130 km corresponding to slit size of 1.2'' × 8.2'' at Δ = 0.19 AU centred on the nucleus of comet C/1996 B2 Hyakutake on 1996 March 30 (Cochran 2008).

TABLE 5  
 CALCULATED GREEN TO RED-DOUBLET EMISSION BRIGHTNESS RATIO AVERAGED OVER  $5'' \times 5''$  SLIT, AT  
 DIFFERENT GEOCENTRIC DISTANCES.

Yield <sup>a</sup> (%)	Geocentric distance (AU)							
	0.1	0.2	0.5	1	1.5	2		
<b>1% CO<sub>2</sub></b>								
0.0	0.11	0.07	0.05	0.04	0.04	0.04	0.04	0.04
0.2	0.17	0.11	0.07	0.06	0.05	0.05	0.05	0.05
0.5	0.26	0.17	0.10	0.08	0.07	0.07	0.07	0.07
1.0	0.40	0.26	0.15	0.12	0.10	0.10	0.10	0.10
<b>0% CO<sub>2</sub></b>								
0.0	0.07	0.05	0.03	0.03	0.03	0.03	0.03	0.03
0.2	0.13	0.09	0.05	0.05	0.04	0.04	0.04	0.04
0.5	0.23	0.15	0.09	0.07	0.06	0.06	0.06	0.06
1.0	0.37	0.24	0.14	0.11	0.01	0.01	0.01	0.01
<b>3% CO<sub>2</sub></b>								
0.0	0.19	0.13	0.08	0.06	0.06	0.06	0.06	0.06
0.5	0.33	0.21	0.13	0.10	0.09	0.09	0.09	0.09

<sup>a</sup>O(<sup>1</sup>S) yield from photodissociation of H<sub>2</sub>O

NOTE.—Calculations are made for 1996 March 30, where  $r=0.94$  AU.

TABLE 6  
 CALCULATED INTENSITIES OF GREEN AND RED-DOUBLET EMISSIONS AND THE G/R RATIO IN COMET  
 C/1996 B2 HYAKUTAKE ON DIFFERENT DAYS OF OBSERVATION IN 1996 MARCH.

Date of observation (1996 March )	r (AU)	$\Delta$ (AU)	$Q_{H_2O}$ ( $s^{-1}$ )	Slit dimension (arcsec)	Projected distance (km)	Calculated 5577 $\text{\AA}$ intensity (kR)	Calculated (6300 + 6364 $\text{\AA}$ ) intensity (kR)	G/R ratio	
								Calculated	Observed
9 <sup>a</sup>	1.37	0.55	$5 \times 10^{28}$	$1.2'' \times 8.2''$	$470 \times 3720$	0.06	0.62	0.09	0.09 <sup>a</sup>
23 <sup>b</sup>	1.08	0.12	$1.8 \times 10^{29}$	7.5'' (circular) <sup>c</sup>	640	0.69	5.88	0.12	0.12 - 0.16 <sup>b</sup>
27 <sup>b</sup>	1.00	0.11	$2 \times 10^{29}$	7.5'' (circular)	653	0.89	7.12	0.12	—
30 <sup>a</sup>	0.94	0.19	$2.2 \times 10^{29}$	$1.2'' \times 8.2''$	$165 \times 1129$	0.90	7.97	0.17	—

<sup>a</sup>Cochran (2008)

<sup>b</sup>Morrison et al. (1997)

<sup>c</sup>7.5'' is the diameter of the circular slit

NOTE.—Calculations are made for O(<sup>1</sup>S) yield of 0.5%, and CO<sub>2</sub> and CO relative abundances of 1% and 22%, respectively.

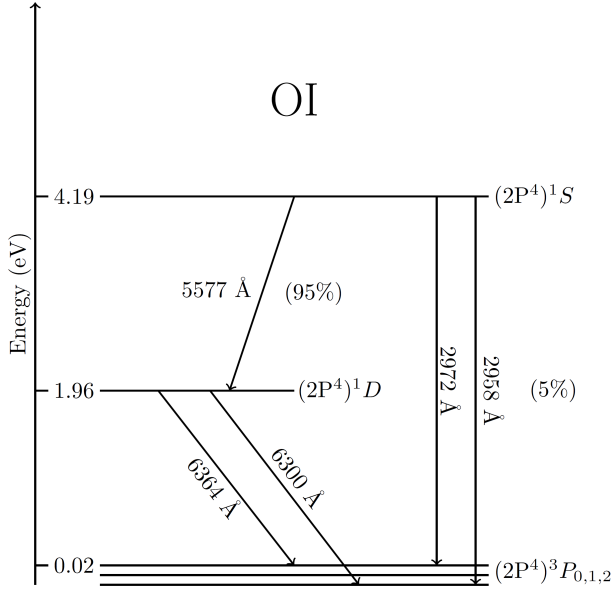


Fig. 1.— Energy level diagram of atomic oxygen showing different spectroscopic transitions related to  $^1S$  and  $^1D$  states.

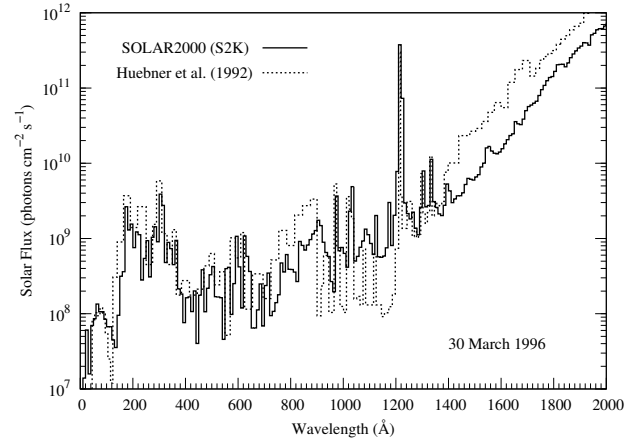


Fig. 2.— Solar EUV-UV flux from SOLAR2000 (S2K) model of Tobiska (2004) for the day 1996 March 30 at heliocentric distance of 1 AU. For comparison the solar flux used by Huebner et al. (1992) is also shown. At H Lyman  $\alpha$  (1216 Å) the solar flux given by S2K model is higher than that of Huebner et al. (1992) by a factor 1.24. Significant differences in the two solar fluxes can be noticed in the wavelength ranges 800 to 1200 Å, while above 1400 Å the solar flux of S2K model is smaller than that of Huebner et al. (1992).

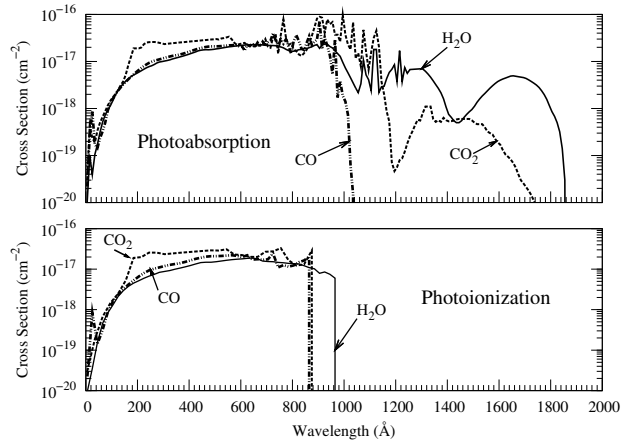


Fig. 3.— The total photoabsorption cross sections for  $H_2O$ ,  $CO_2$  and  $CO$  are shown in the top panel and total photoionization cross sections are shown in the bottom panel. The cross sections are taken from Huebner et al. (1992).

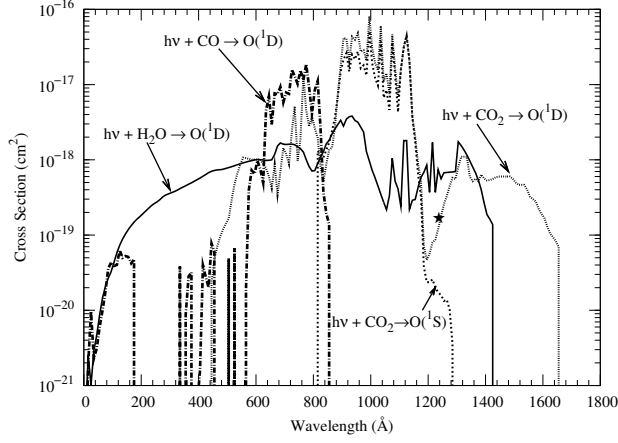


Fig. 4.— Photodissociative excitation cross sections for the production of  $O(^1D)$  from  $H_2O$ ,  $CO_2$ , and  $CO$ . These cross sections are taken from Huebner et al. (1992). ★ represents the cross section value for the production of  $O(^1S)$  from  $H_2O$  at 1216 Å assuming 1% yield.

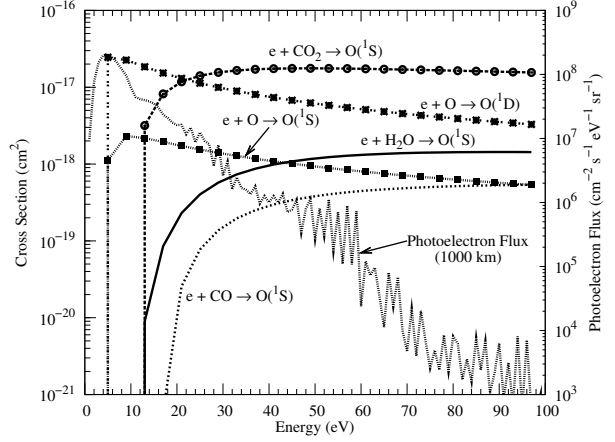


Fig. 5.— Cross sections for the production of metastable  $O(^1S)$  in electron impact dissociative excitation of  $H_2O$ ,  $CO_2$ , and  $CO$ . Cross sections for electron impact excitation of  $O$  to  $O(^1D)$  and  $O(^1S)$  are also plotted. Calculated steady state photoelectron flux at 1000 km cometocentric distance using S2K model solar flux on 1996 March 30 is also shown with scale on right side y-axis.

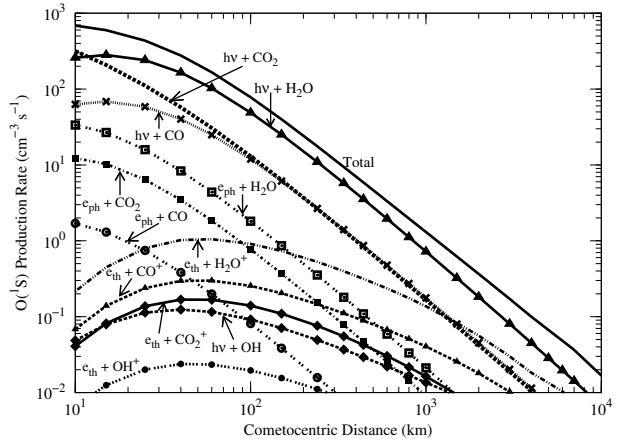


Fig. 6.— Calculated radial profiles for major production mechanisms of  $O(^1S)$  along with the total production profile.  $h\nu$  = solar photon,  $e_{ph}$  = photoelectron, and  $e_{th}$  = thermal electron.



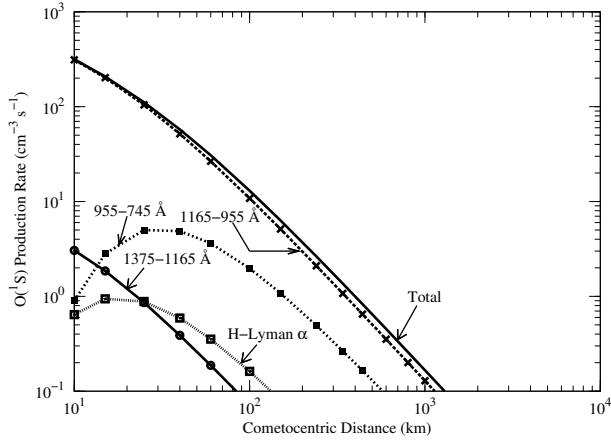


Fig. 7.— Calculated radial profiles for the photodissociation of  $\text{CO}_2$  producing  $\text{O}(^1\text{S})$  at different wavelength bands.

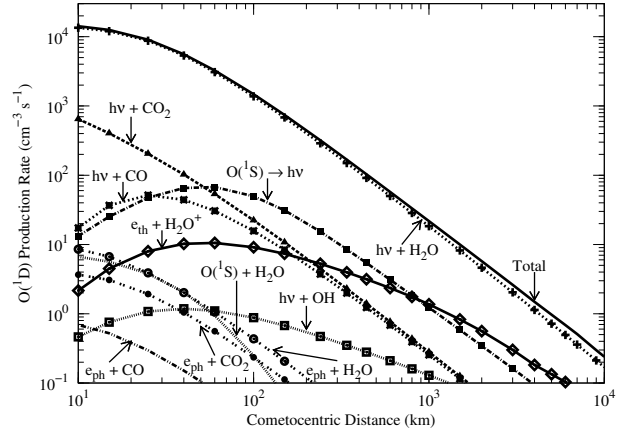


Fig. 9.— Calculated radial profiles for the major production mechanisms of  $\text{O}(^1\text{D})$  along with total  $\text{O}(^1\text{D})$  production rate profile.  $h\nu$  = solar photon,  $e_{ph}$  = photoelectron, and  $e_{th}$  = thermal electron.

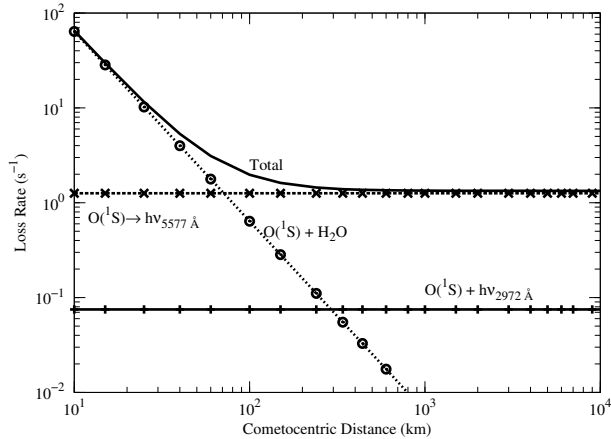


Fig. 8.— Calculated radial profiles for the major loss mechanisms of  $\text{O}(^1\text{S})$  atom.

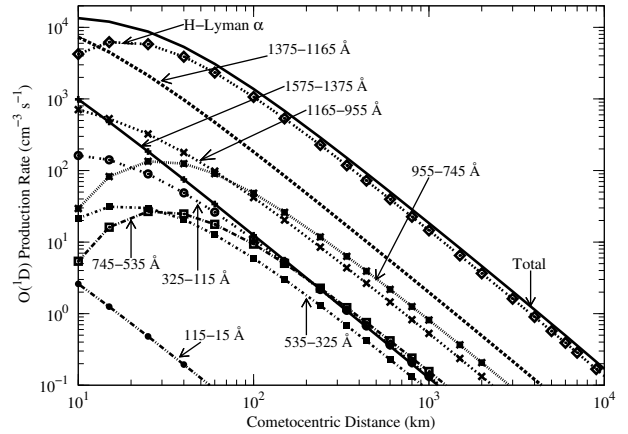


Fig. 10.— Calculated radial profiles for the photodissociation of  $\text{H}_2\text{O}$  producing  $\text{O}(^1\text{D})$  at different wavelength bands.

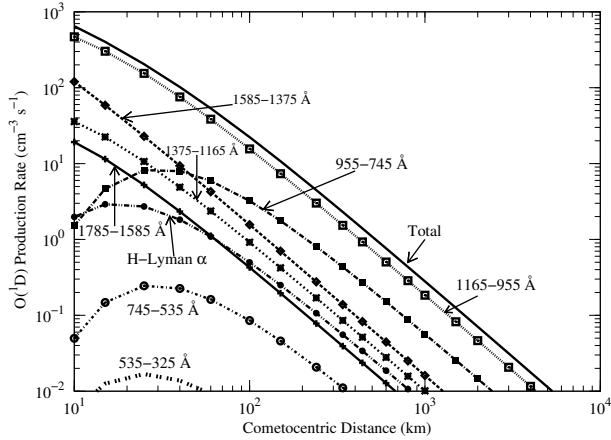


Fig. 11.— Calculated radial profiles for the photodissociation of  $\text{CO}_2$  producing  $\text{O}(^1\text{D})$  at different wavelength bands.

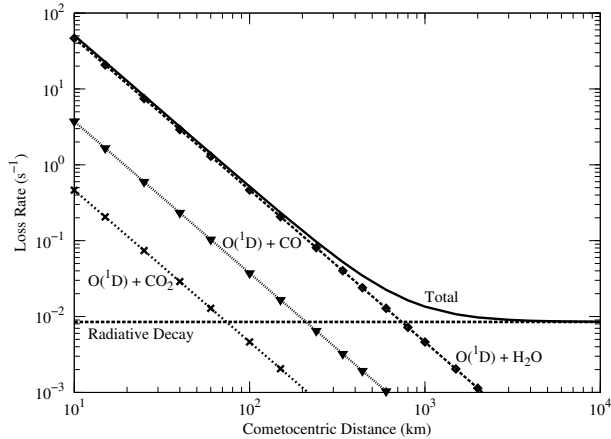


Fig. 12.— Calculated radial profiles for major loss mechanisms of  $\text{O}(^1\text{D})$  atom.

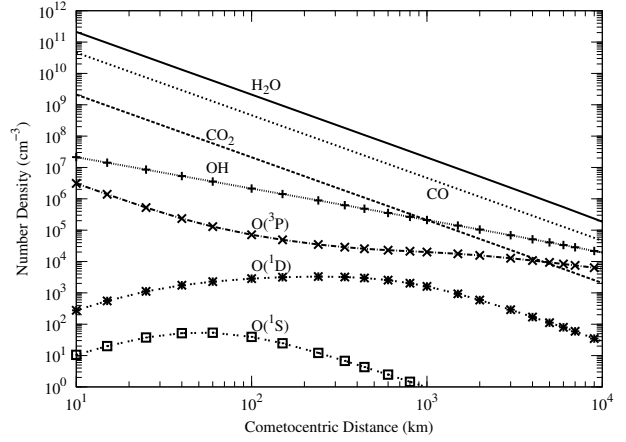


Fig. 13.— Calculated number density profiles of  $\text{O}(^1\text{S})$ ,  $\text{O}(^1\text{D})$ ,  $\text{O}(^3\text{P})$ , and  $\text{OH}$ , along with those of  $\text{H}_2\text{O}$ ,  $\text{CO}$ , and  $\text{CO}_2$ .

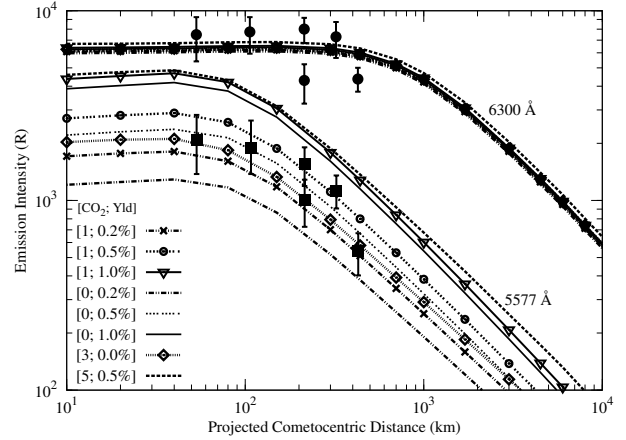


Fig. 14.— Calculated emission brightness profiles along projected distances for 5577 Å (green) and 6300 Å (red) line emissions for different  $\text{CO}_2$  relative abundance  $[\text{CO}_2]$  and yield  $[\text{Yld}]$  for  $\text{O}(^1\text{S})$  production in photodissociation of  $\text{H}_2\text{O}$ . The green and red emission intensities at different projected distances observed on March 30 taken from Cochran (2008) are also shown (filled symbols with error bars) for comparison with the calculated values.

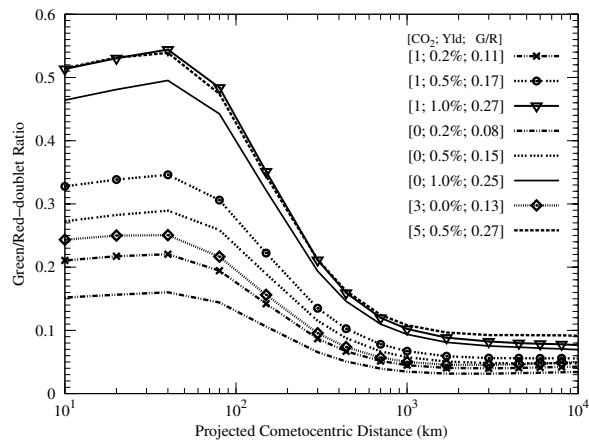


Fig. 15.— Calculated green to red-doublet intensity ratio along projected distances for different  $\text{CO}_2$  relative abundance  $[\text{CO}_2]$  and yield  $[\text{Yld}]$  for  $\text{O}(^1\text{S})$  production in photodissociation of  $\text{H}_2\text{O}$ .  $\text{G/R}$  = calculated green to red-doublet intensity ratio averaged over slit projected size  $165 \times 1130$  km for C/1996 B2 Hyakutake on 1996 March 30.